Optical Spatial Solitons for All-Optical Signal Processing

Armando Piccardi

Department of Electronic Engineering

University of Rome "ROMA TRE"

A thesis submitted in partial fulfillment
of the requirements for the degree of

Doctor of Philosophy

2010

CORSO DI DOTTORATO

in

INGEGNERIA ELETTRONICA:
DALLE NANOSTRUTTURE AI SISTEMI
XXI CICLO

Supervisor:

Prof. Gaetano Assanto

PhD course - coordinator:

Prof. Giuseppe Schirripa Spagnolo

To my father

Acknowledgements

I am grateful to all the people who supported me during these years.

First of all I thank Prof. Gaetano Assanto for giving me the opportunity to work in a stimulating environment and for disclosing me the trail towards research. I also thank Dr. Marco Peccianti for guiding me along the first steps of the world of liquid crystals, with his competence and helpful discussions. A special thank to Dr. Alessandro Alberucci for his collaboration, his advice and his help through the theoretical aspects of the problems I faced.

I also thank Dr. Stefania Residori and Dr. Umberto Bortolozzo who hosted me in INLN for their constant attention to my work there.

Thanks to Prof. Francesco Simoni, Dr. Liana Lucchetti, Dr. Andriy Dyadyusha and Dr. Malgosia Kaczmarek for providing some of the samples used in my experiments.

I thank all my labmates of these years for their help and friendship during all the breaks, launches, dinners and beyond. In mere alphabetical order: Alessia, Andrea, Andrea, Elena, Florence, Jisha, Lorenzo, Michele, Raouf, Salvatore, Schirin, Usman, Vito.

And I also want to thank the other guys whom I spent these years with, the new friends and the old ones, for helping me to find new answers to my questions, together with new questions.

A very special thank goes to Marta, for simply being who she is.

Last, but not least, I will always be indebted to my family: without them none of this would have been possible.

Thank you all.

Abstract

Nonlinear systems respond to an excitation in a non-proportional way and do not satisfy the superposition principle. Most of the linear models of physical systems (harmonic oscillator is probably the clearest example) are valid approximations only in a perturbative regime; beyond it their intrinsic nonlinear nature must be considered. The nonlinear world is a source of intriguing phenomena (both from theoretical and applicative points of view) and optics is one of the most accessible area where such effects can be studied. When light and matter interact, the former is able to change the medium properties, in particular the refractive index, so affecting its own propagation. Among the nonlinear processes we will consider self-confinement: the ability of a light beam to compensate its natural tendency to spread. When linear spreading is exactly compensated by non-linear self-focusing, a spatial soliton is formed. Spatial solitons preserve their profile during propagation, which makes them suitable candidates to carry and process other signals, just like waveguides. We will deal with spatial solitons in nematic liquid crystals, namely *nematicons*, in which nonlinearity is enabled by dipolar interactions between molecules and electric fields: the material is chosen on the basis of its high nonlinearity and versatility. This dissertation reports on the all-optical control of nematicons and some representative applications of signal processing. The work is mostly experimental, with some theoretical considerations wherever it is necessary for the comprehension of the observed phenomena.

Chapter 1. Fundamentals of nonlinear optics and spatial solitons are firstly summarized. Then we examine Nematic Liquid Crystals and their physical properties, focusing the attention on their nonlinear optical response and introducing nematicons.

Chapter 2. We report some experiments in standard samples. First, we examine the propagation of a nematicon in the presence of a tunable nonlinearity. Then we treat the nonlinear control of the interaction between two nematicons.

Chapter 3. Here we present experiments in dye-doped liquid crystals. We describe the optical response of dye-doped nematics and two experiments. In the first, we discuss nonlinear self-steering of light, comparing undoped and doped liquid crystals; in the second we deal with the formation of optical interfaces in order to control the nematicon trajectory.

Chapter 4. We introduce liquid crystal light valve as a novel environment for the propagation of nematicons. After a preliminary section where we explain the working principles of the valve, we illustrate the propagation of a nematicon in a fully controllable refractive index landscape. We review briefly the theorical approach, proposing and demonstrating the implementation of a reconfigurable set of all-optical signal processors.

Contents

List of Figures

1

Introduction

1.1 Nonlinear optics

The study of light-matter interactions has acquired great importance in modern science, as it allows both the comprehension of fundamental physical processes and their exploitation in optical communication and signal processing. In particular, nonlinear optics is undoubtly one of the most fascinating field in optics, as it discloses a large number of intriguing mechanisms for light manipulation. The term *"nonlinear"* refers to the relationship between an electric field $\boldsymbol{E}$ propagating in a medium and the polarizability vector $\boldsymbol{P}$: this link is usually assumed to be linear, through $\mathbf{P} = \epsilon_0 \overline{\chi}^{(1)} \mathbf{E}$ (where ϵ_0 is the vacuum dielectric constant and $\overline{\chi}^{(1)}$ is the electric susceptibility), as it comes from first order approximation. Considering higher order terms:

$$\mathbf{P} = \epsilon_0 \left(\overline{\chi}^{(1)} + \overline{\overline{\chi}}^{(2)} \mathbf{E} + \overline{\overline{\overline{\chi}}}^{(3)} \mathbf{E}^2 + \dots \right) \mathbf{E} \tag{1.1}$$

where $\overline{\chi}^{(1)}$, $\overline{\overline{\chi}}^{(2)}$ and $\overline{\overline{\overline{\chi}}}^{(3)}$ are first-, second- and third-rank tensors, respectively.

In most common materials, higher order coefficients are usually negligible, so that nonlinearity becomes appreciable only at very high intensities; moreover, considering them is an involved theoretical problem and requires hard computation. It is for these reasons that nonlinear optics was born in the '50s, when the pioneering work of Fermi, Pasta and Ulam discussed through numerical simulations the energy distribution between the modes of a vibrating string. (1) The intensities needed for experimentally explore nonlinear materials became available in the '60s with the invention of laser, and in the 1961 the first example of frequency conversion was reported. (2) Among

the various classes of nonlinear optical phenomena discovered in the late sixties, light confinement has been widely investigated for its general character. In 1964, Chiao *et al* showed firstly the possibilities to compensate linear diffraction, (3) while in 1970, Grischkowsy experimentally demonstrated nonlinear self-focusing in Potassium vapor. (4) Three years later Bjorkholm and Ashkin observed the first optical spatial soliton. (5)

1.2   Solitons

The pioneering observation of a soliton is attributed to John Scott Russell in 1834, when he reported about a *"wave of translation"* looking at a water wave propagating in a channel.

"...I was observing the motion of a boat which was rapidly drawn along a narrow channel by a pair of horses, when the boat suddenly stopped - not so the mass of water in the channel which it had put in motion; it accumulated round the prow of the vessel in a state of violent agitation, then suddenly leaving it behind, rolled forward with great velocity, assuming the form of a large solitary elevation, a rounded, smooth and welled -defined heap of water, which continued its course along the channel apparently without change of form or diminution of speed. I followed it on horseback, and overtook it still rolling on at a rate of some eight or nine miles an hour, preserving its original figure some thirty feet long and a foot to a foot and a half in height. Its height gradually diminished, and after a chase of one or two miles I lost it in the windings of the channel. Such, in the month of August 1834, was my first chance interview with that singular and beautiful phenomenon which I have called the Wave of Translation..." (6).

Analyzing Russel's careful description, we find that first he noticed the phenomenon was generated by a strong excitation; then he recognized the peculiar shape of the wave and, finally, its tendency to preserve it. In other words, he observed that, under appropriate conditions, a medium can support the propagation of shape-invariant waves. More specifically, this behavior is due to a self-action of the wave, mediated by its interaction with the medium. This kind of shape-preserving waves are called *solitons*. (7)

Different classes of solitons can be found in nature in all branches of physics, including optics [7][8][9], chemistry [10][11], hydrodynamics [12] and plasma physics. [13][14][15] Though nonlinear mechanisms are physically different, they always arise when a natural wave spreading is counterbalanced by nonlinear effects. From a mathematical point of view, solitons are solutions of a class of dispersive nonlinear equations [16]: one of the most studied, and the one that will be treated in the following sections, is the *Non Linear Schrödinger Equation* (NLSE) [17], which in (1+1)D reads:

$$i\frac{\partial u}{\partial q} + \frac{1}{2}\frac{\partial^2 u}{\partial p^2} \pm f\left(|u|^2\right)u = 0 \tag{1.2}$$

where u is the vectorial field under investigation, q the propagation coordinate, p the transverse coordinate and f a general nonlinear function modeling the medium response.

1.2.1 Optical Solitons

Let us consider an electric field u associated to a light beam, i.e. optical soliton propagation. [18][9][19] With reference to eq. 1.2, a first classification is based on the coordinate in the first term: if q is time, we deal with optical pulses experiencing dispersion. In this case we talk of *temporal solitons*; if q is a spatial coordinate, we consider light diffraction, i.e. *spatial solitons*. Depending on the sign of the last term, we distinguish between *bright* and *dark* solitons. The former (sign +) is related with a *focusing* nonlinearity, with the soliton given by a bell shaped function; the latter (sign -) represents a *defocusing* medium and the soliton profile is given by a dip in a constant background, encompassing a transversal π phase. [20] A further classification can be made on the basis of the function *f*. In optics it defines the refractive index and in the nonlinear case it describes the light-matter interaction and represents an intensity dependent refractive index: the medium response can be punctual and is said to be *local*, while if the perturbation extends well beyond the beam the medium is *nonlocal*. The latter case is of a crucial importance because *nonlocality*, stabilizes soliton solutions in 2D problems and mediates soliton interactions. [8][21][22][23] If a linear relationship between nonlinear variations of the refractive index and intensity

and transversal invariance are assumed, f can be expressed as:

$$f = \int G(\mathbf{r} - \mathbf{r'}) \left| u(\mathbf{r'}) \right|^2 d\mathbf{r'} \tag{1.3}$$

where $G(\mathbf{r} - \mathbf{r'})$ is the *Green function* modeling the medium response.

Integrable solutions of eq. 1.2 can be found if f is linear and local, i.e. in a pure Kerr media (3); in such case eq. (1.2) becomes a standard NLSE, which can be solved by *inverse scattering transform.* (16) In fact, if $f = |u|^2$ and taking u as $u = a(p)e^{i\phi(p,q)}$, *inverse scattering* leads to the expression for the fundamental soliton solution in the form $u = \frac{a}{\cosh(aq)}e^{ia^2q/2}$ for a *bright* soliton or $u = a \tanh(ap)e^{ia^2q/2}$ for a *dark* one. (20) In general, finding closed form solutions is impossible; for highly nonlocal media it is possible to approximate the index perturbation with a parabolic potential and use the well known solution for the harmonic oscillator; hence, the soliton profile is gaussian and can be describes by a particle-like behavior. (24)(25)(26)

Suitable conditions for self-focusing are thus strongly dependent on the nonlinear response, i.e. on the function f: Kerr (5), $\chi^{(2)}$ (27), thermal (28)(29) photorefractive (30) and reorientational (31) materials have been well studied in the past years. In the following we will focus on *highly nonlocal bright optical spatial solitons* propagating in *nematic liquid crystals.* (32)

1.3 Liquid Crystals

The liquid crystalline phases are intermediate between solid and liquid, with intermolecular forces unable to sustain a long range order. (33) Thermotropic liquid crystals are the most widely used and can be classified depending on the type of molecular order: nematic, smectic and cholesteric.

The *Nematic phase* is characterized by no positional order but a certain degree of orientational order along the optic axis ("director").

The *Smectic phase* possesses both positional and orientational order, the latter only along one direction; the intermolecular structure resembles a stratified medium.

The *Cholesteric phase* is similar to the nematic one but with a twisted molecular orientation.

We will deal with *Nematic Liquid Crystals.*

1.3.1 Nematic Liquid Crystals

Nematic Liquid Crystals (NLC) (34)(35) are organic compounds consisting of elongated molecules (the Greek word *nematos* indicates a *thread*) with a roughly rod-like symmetry. Orientational order allows to identify a mean direction for the long axis, associated to the vector *molecular director*, indicated by $\boldsymbol{n}$. Due to relatively small intermolecular forces (of the same order of magnitude of thermal agitation) a critical temperature T_{NI} separates the nematic phase, possessing an (orientationally) ordered structure at microscopic level, from the isotropic phase, where molecules are randomly arranged (see fig. 1.1).
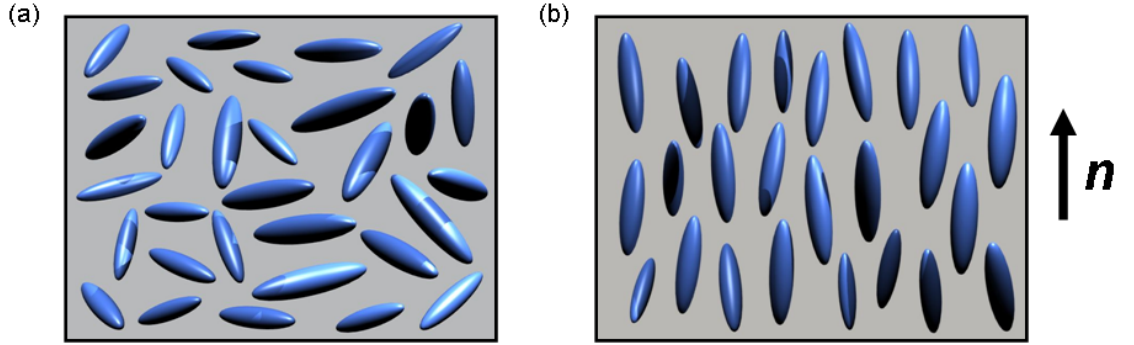
Figure 1.1: NLC molecular arrangement (molecules are sketched as blue ellipses). (a) Isotropic phase: molecules are randomly arranged in space. (b) Nematic phase: orientational order determines a specific direction of molecular director.

1.3.1.1 Optical properties

Let us consider a plane wave with a propagating wavevector $\boldsymbol{k}$ in a homogeneous NLC sample (this can be obtained by imposing a long range order with suitable interface treatment). As NLC exhibits two different refractive indices associated to the directions parallel and perpendicular to $\boldsymbol{n}$, respectively $n_{\parallel} = \sqrt{\epsilon_{\parallel}}$ and $n_{\perp} = \sqrt{\epsilon_{\perp}}$ [see fig. 1.3(a)] with typically $n_{\parallel} > n_{\perp}$, we can consider the macroscopic behavior of NLC as equivalent to a positive uniaxial of anisotropy $\epsilon_a = \epsilon_{\parallel} - \epsilon_{\perp}$ and optic axis $\boldsymbol{n}$. Thus, the dielectric tensor components are expressed by $\epsilon_{ij} = \epsilon_{\perp}\delta_{ij} + \epsilon_a n_i n_j$, where δ_{ij} is the Kronecker's delta and $n_{i,j}$ the director components. For a generic direction of the optic axis, the

ordinary refractive index $n_o = n_\perp$, whereas the extraordinary one n_e depend on the angle θ between $\boldsymbol{n}$ and $\boldsymbol{k}$:

$$n_e = \frac{n_\parallel n_\perp}{\sqrt{n_\parallel^2 \cos^2 \theta + n_\perp^2 \sin^2 \theta}}. \tag{1.4}$$

The large birefringence ($\Delta n = n_\parallel - n_\perp \approx 0.2$) causes the Poynting vector $\boldsymbol{s}$ to propagate at a not negligible *walk-off* angle δ with respect to $\boldsymbol{k}$, being $\tan \delta = \epsilon_{yz}/\epsilon_{zz}$, so that:

$$\delta = \arctan \left[\frac{\epsilon_a \sin 2\theta}{2\epsilon_\perp + \epsilon_a (1 + \cos 2\theta)} \right]. \tag{1.5}$$
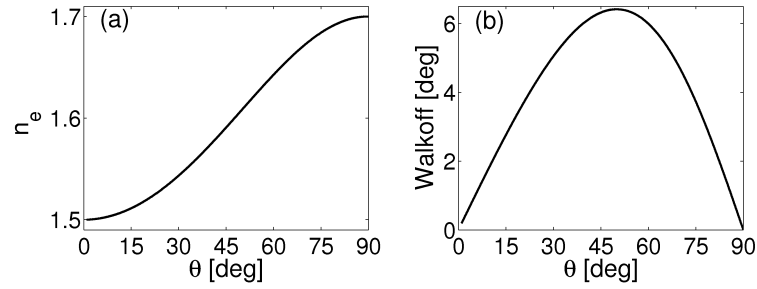
Figure 1.2: (a) Extraordinary refractive index and (b) walk-off angle versus angle θ. Typical values are considered for $n_\parallel$ (1.7) and $n_\perp$ (1.5).

The above properties are valid in the linear regime. If we consider the microscopic molecular response to electric fields, at both low and optical frequencies, we discover that the interaction induces a molecular dipole along $\boldsymbol{n}$ and a mechanical torque which tends to align the molecules parallel to the field [fig. 1.3(b),(c)].

The equilibrium condition is reached when the electrically induced torque is balanced by the elastic intermolecular forces. The formal description of the NLC response to external excitations was introduced by De Gennes (33) and is known as *continuum theory*.

1.3.1.2 Continuum theory and reorientation equation

When an external electromagnetic excitation interacts with NLC, the torque modifies the director distribution until a new equilibrium condition is reached. This can be found by calculating the energy due to the field-induced director distortion and minimizing
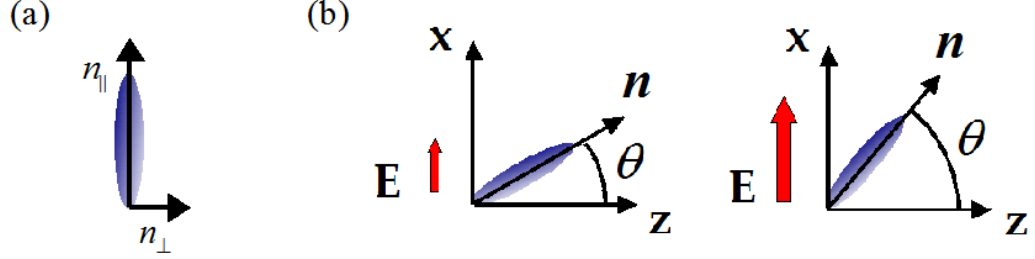
Figure 1.3: NLC optical properties. (a) The NLC anisotropy is given by the difference in the refractive indices associated to direction parallel and perpendicular to the long axis (molecular director), $n_\parallel$ and $n_\perp$, respectively. (b) When interacting with an electric field $\boldsymbol{E}$, molecules reorient towards the field direction, the angle θ being dependent on the field intensity.

it. Under strong anchoring conditions at the sample boundaries, the induced torque can be expressed by $F_E = \frac{\epsilon_a}{2} \left(\boldsymbol{n} \cdot \boldsymbol{E}^2 \right)$, while the elastic energy is:

$$F_r = \frac{1}{2} \left\{ K_1 \left(\nabla \cdot \boldsymbol{n} \right)^2 + K_2 \left(\boldsymbol{n} \cdot \nabla \times \boldsymbol{n} \right)^2 + K_3 \left[\boldsymbol{n} \times \left(\nabla \times \boldsymbol{n} \right) \right]^2 \right\} \tag{1.6}$$

where K_1, K_2 and K_3 are the Frank elastic constants for splay, twist and bend distortions, respectively. For planar deformations ($K_2 = 0$) and a single constant approximation ($K_1 \approx K_3 = K$), Euler-Lagrange equations lead to the *reorientation equation* (34)

$$K \nabla^2 \theta + \frac{\epsilon_0 \epsilon_a}{2} \sin 2\theta \left| E \right|^2 = 0 \tag{1.7}$$

1.4   Spatial Solitons in Nematic Liquid Crystals

In this section we analyze the main features of the propagation of spatial solitons in NLC. First we describe the sample geometry and the experimental set-up used in the following chapters; then we illustrate the propagation of this kind of solitons. Finally, we present the ruling model.

1.4.1   Geometry of the NLC cell

With reference to fig. 1.4, a liquid crystal cell is composed by two glass slides containing an NLC layer. A third orthogonal glass, employed as input interface, seals the cell,

7
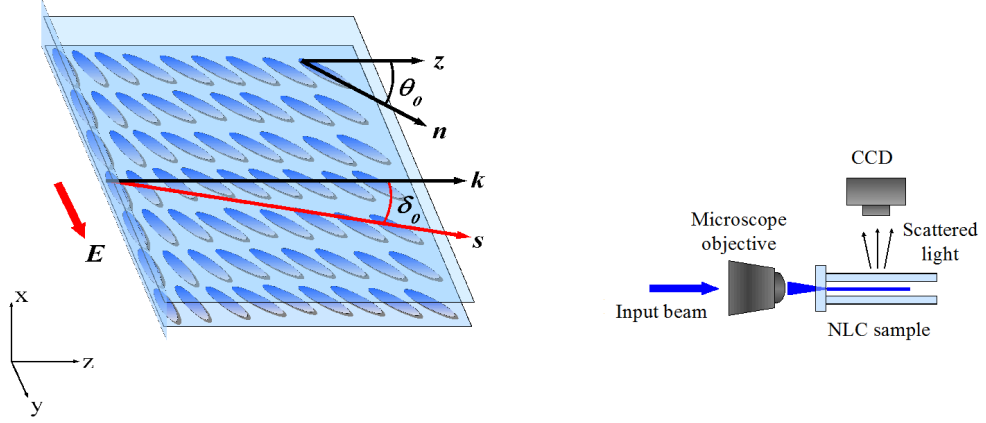
Figure 1.4: Sketches of a NLC cell and of the experimental set-up

avoiding meniscus formation and depolarization effects. Surfaces treatment aligns the molecular director in a specified direction inside the cell at an angle θ_0, as in fig. 1.4: this forces the NLC to have a long-range order even in the bulk. Two kinds of anchoring are feasible: planar and homeotropic; the former (the one we will deal with in the rest of the work) forces the director to lay parallel to the surface, its direction being determined during the technological process, the latter forces it to be perpendicular. The orientation at the input facet is chosen to optimize the coupling of extraordinarily polarized beams. (36)

To perform the experiments a laser beam is focused to a waist of a few microns at the input facet in the middle of the cell thickness, to avoid undesired interactions with the cell boundaries. (37)(38)(39) The beam evolution can be monitored by collecting the out-of-plane scattered light with a microscope and a high resolution CCD camera, yz being the observation plane.

1.4.2 Nematicons

Let us consider a fundamental gaussian beam propagating in an NLC sample with wavevector $\boldsymbol{k}$ directed along z. With reference to fig. 1.4, the long molecular axis is in the yz plane at an angle θ_0 with z. All-optical reorientation will occur in the yz plane. As for plane waves, the ordinary beam component propagates straight, while the Poynting vector of the extraordinary wave will be directed along $\boldsymbol{s}$, in general different
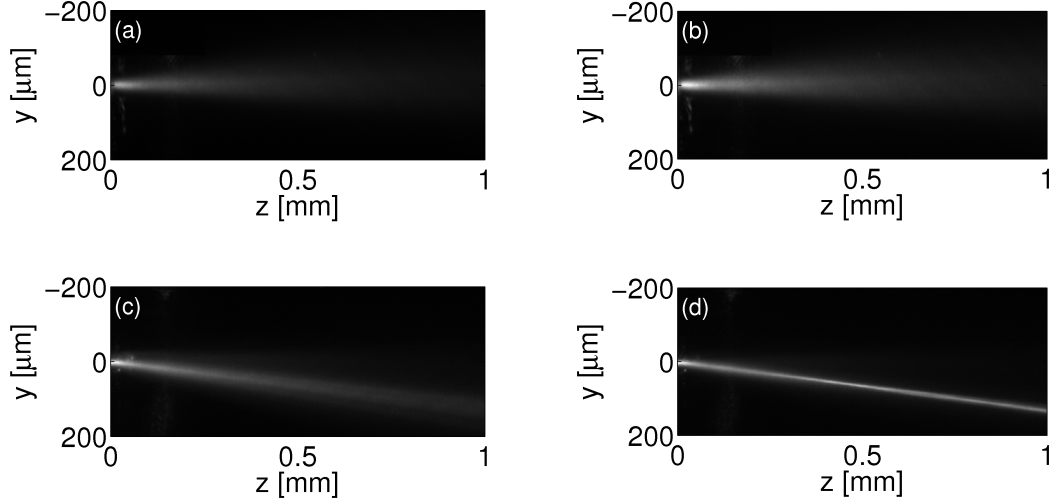
Figure 1.5: Beam propagation in NLC. The ordinary component propagates straight and diffracts both at (a) $P = 0.7mW$ and at (b) $P = 2mW$ due to Freedericksz's threshold. Energy propagation of the extraordinary component is rotated by the walk-off angle and the beam diffracts for (b) $P = 0.7mW$ while reorientational nonlinearity enables the formation of a *nematicon* for (d) $P = 2mW$. In the pictures a beam at $\lambda = 1.064\mu m$ from a Nd:YAG laser is focused to a waist of $\approx 5\mu m$ into E7 NLC ($n_\parallel \approx 1.7$ and $n_\perp \approx 1.5$). $\theta_0 = 45°$ and correspondingly $L_r \approx 120\mu m$ and $\delta \approx 7°$.

from z by δ. In the linear regime [fig. 1.5(a),(c)] both beam components diffract with their characteristic Rayleigh length $L_r = n_{o/e}\pi w_0^2/\lambda$, with w_0 the input beam waist.

The ordinary component (electric field along x) does not have an intensity dependent behavior [fig. 1.5(a),(b)], as the Freedericksz's threshold (33) prevents reorientation (torque is null). For the extraordinary polarization ($\boldsymbol{E} \in yz$) the Freedericksz's threshold is zero and light of sufficient intensity (namely $\approx 1mW$) (40) can reorient the director towards the field vector; the director rotation causes the effective refractive index $n_e(\theta)$ to increase. (41)(42) As a consequence, the NLC part perturbed by the beam will act as a focusing lens. When this nonlinear self-focusing balances linear diffraction, the solitonic regime is reached [fig. 1.5(d)]. We will also refer to a spatial soliton in NLC as a *nematicon*. (32) Due to the elastic forces, the index perturbation is much wider than the beam width (see eq. (1.9)) (25)(26)(43): this prevents catastrophic collapse and stabilizes nematicons. As the power dependent behavior relies on molecular rotation until $\boldsymbol{n}$ is parallel to the applied field, NLC is said to exhibit a *saturable reorientational nonlinearity*. (25)(31)

9

1.4.3 Ruling equations

The model describing this mechanism can be obtained from Maxwell's equations under the paraxial approximation and accounting for the medium anisotropy; a *Schrödinger-like* equation describes the field evolution inside NLC. The nonlinearity is accounted for by considering the relationship between the refractive index and the field intensity through molecular reorientation. The ruling equations we employ in this work are:

$$2ik_0n_e\left(\frac{\partial A}{\partial z} + \tan\delta\frac{\partial A}{\partial y}\right) + D_x\frac{\partial^2 A}{\partial x^2} + D_y\frac{\partial^2 A}{\partial y^2} + k_0^2\Delta n_e^2 A = 0 \qquad (1.8)$$

$$\nabla^2\theta + \kappa\sin\left[2\left(\theta - \delta\right)\right]|A|^2 = 0 \qquad (1.9)$$

where z is the propagation direction, x and y the two transverse coordinates, A the fields envelope, δ the walk-off, D_x and D_y the diffraction coefficients, $\Delta n_e^2 = \sin^2\left(\theta - \delta\right) - \sin^2\left(\theta_0 - \delta\right)$, θ the optically perturbed angle, θ_0 the initial angle between $\boldsymbol{n}$ and $\boldsymbol{k_0}$, $\kappa = \epsilon_0\epsilon_a/4K$, ϵ_0 the vacuum dielectric constant, ϵ_a the optical anisotropy and K the Frank constant in the single constant approximation. (35)

The first term in eq. (1.8) (NLSE) rules the propagation features: owing to anisotropy the walk-off is considered. Second and third terms account for diffraction in 2D. The last term is the equivalent potential: the light induced refractive index change is linked to the angular variation of the molecular director. This relationship is explicitated through eq. (1.9) (reorientation equation), expressing the balance between the induced torque and the elastic response. (25)

1.5 Aim of the work

The nature of self-induced waveguides makes nematicons capable of guiding other copolarized signals; thanks to their robustness when interacting with director distortions, they can be employed as basic elements of readdressable interconnects for signal processing. Soliton control in NLC has been demonstrated with the use of external voltages (44)(31), interactions with other self-confined beams (23)(45) or induced defects in director alignment (46)(47) and electrically driven interfaces. (48)(49)(50)

In this thesis I propose some strategies for all-optical signal processing based on nematicons: all the illustrated phenomena will focus on applications to processing, routing and demultiplexing.

2

Nematicons and their interactions

In the previous chapter we illustrated how to excite solitons in NLC, enlightening their basic properties as well as the theoretical and experimental tools to study their behavior. In this chapter we will discuss the role of nonlinearity and nonlocality in nematicon propagation: we will show how nonlinearity can affect soliton propagation in a custom designed cell and how nonlocality mediates soliton-soliton interactions.

2.1   Tunable nonlinearity in NLC

With reference to eq. 1.8, it is clear that the nonlinear term depends on the angle θ_0 through eq. 1.9: in a NLC cell it sets the initial *background* angle, defining both the extraordinary refractive index as well as the magnitude of the all-optical response; hence, a careful choice of this value customizes the cell for a specific experiment.

We can evaluate an equivalent nonlinear parameter n_{2eq}: as in eq.(1.8) $\Delta n_e^2 = n_e^2(\theta) - n_e^2(\theta_0)$, we can write $\Delta n_e^2 = 2\Theta(|A|^2)n_e(\theta_0)\partial n_e/\partial\theta$. From eq. (1.9), in the limit of low optical perturbation, $\Theta(|A|^2)$ can be found solving a *Poisson's-like* equation; the expression of $\partial n_e/\partial\theta$ comes from the direct derivation of eq. 1.4. The final expression for the equivalent nonlinearity is:

$$n_{2eq}(\theta_0) \simeq 2\kappa \sin\left[2(\theta_0 - \delta_0)\right] n_e(\theta_0) \left.\frac{\partial n_e}{\partial\theta}\right|_{\theta=\theta_0} \tag{2.1}$$

As also shown in fig. 2.3(e), the maximum of the curve is positioned around $\theta_0 = \pi/4$. This means that to maximize the nonlinearity we need an initial director at that θ_0. Even if this seems the optimum condition (and in almost all cases it is), there are cases in which the highest nonlinearity is not the priority; hence, we need to study how nematicon propagation is affected by initial angular conditions. Despite of the knowledge of eq. (1.8), it is not trivial to find a solution taking into account the term θ_0 and the nematicon properties depending on it. The theoretical model leads to closed forms solutions for the waist behavior in the highly nonlocal limit (24)(26). Furthermore, in previous geometries variations of the nonlinearity were coupled with changes in nonlocality. (51) Unfortunately, the standard cell technology allows fabricating samples with fixed initial director: comparisons between different samples are inappropriate due to the difficulty in reproducing identical experimental conditions, either for the unavoidable fabrication defects (non uniform anchoring at surfaces, losses on input interface) or for experimental inaccuracy in coupling light in the NLC samples.

2.1.1 Biased samples

A varying nonlinearity can be obtained by applying a low frequency electric field between the cell surfaces: the application of a bias is widely used in NLC cells, both to overcome the Freedericksz's threshold (40) or to create electrically induced interfaces or potentials. (49) To favor sample biasing, a layer of Indium Tin Oxide (ITO) transparent electrode is deposited on each inner surface of the cell. In a planar cell the application of a voltage produces molecular orientation in the plane defined by the electric field polarization and $\boldsymbol{n}$, as shown in fig. 2.1: due to the anchored molecules which are not allowed to rotate, an electrically induced equivalent *potential well* is established in the sample, with its center at $x = h/2$. In this way we can tailor the initial director distribution, changing at the same time both nonlinearity (directly through $\boldsymbol{n}$) and nonlocality (through the potential shape). (51)

On one hand this gives versatility to the samples, on the other hand it has some detrimental effects: for high enough voltages, the nonlinearity can saturate due to large reorientation and the nonlocality can vary due to the anchoring conditions. Moreover, the director rotation shifts the walk-off out of the propagation plane yz, towards the cell boundaries, causing beam bouncing at the surface(s) (52) and preventing a "clean" evaluation of the nematicon propagation.
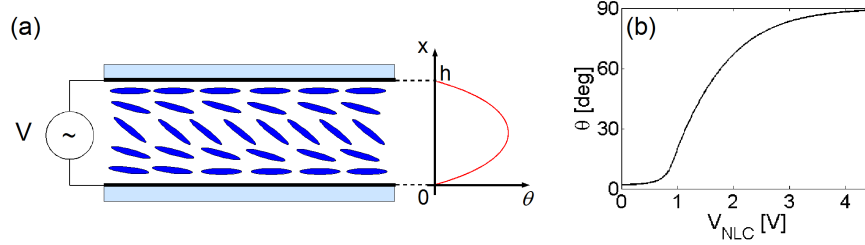
Figure 2.1: (a) Sketch of a NLC biased cell and the corresponding electrically induced potential. (b) Reorientation angle versus applied voltage.

2.1.2 Sample configuration

To overcome these problems, a customized sample was designed. A planar cell of thickness $h = 100\mu m$ was prepared with interfaces ensuring molecular anchoring at $\theta_0 = 80°$ with respect to the z-axis (and to the wavevector $\boldsymbol{k}$ of the injected beams), as sketched in fig. 2.2(a). ITO electrodes were deposited on each interface (top and bottom) with a double comb layout, the two structures connected to distinct biases and interdigitated [fig. 2.2(b)]. Each tooth was orthogonal to z and $\Lambda/4 = 15\mu m$ thick, periodically spaced by $\Lambda/2 = 30\mu m$, so that the distance between teeth of the same comb was $\Lambda = 60\mu m$ [fig. 2.2(c)]. The sample was filled with commercial E7.

Since the distance $\Lambda/2$ is much smaller than the cell thickness, the x-component of the applied electric field assumes significant values only in the proximity of the surfaces where the NLC is anchored and near the electrodes edges, being averaged out by the nonlocal response elsewhere. Hence, the dominant component of the electric field is parallel to z along the cell, nearby the surfaces. The overall Coulombian torque reorients the director $\boldsymbol{n}$ in $x = \pm h/2$ enabling, through intermolecular forces, electrically induced molecular reorientation in the plane yz.

2.1.3 Experimental results

As pointed out in the previous chapter, since the nonlocal character of eq. (1.8) prevents the occurrence of a critical power for soliton formation, guided wave modes exist over a large range of intensities: in this environment light experiences a distributed lens-like behavior of the medium, with a continuous competing action between spreading and confinement. As a consequence, *breathing* solitary waves, i.e. confined beams with
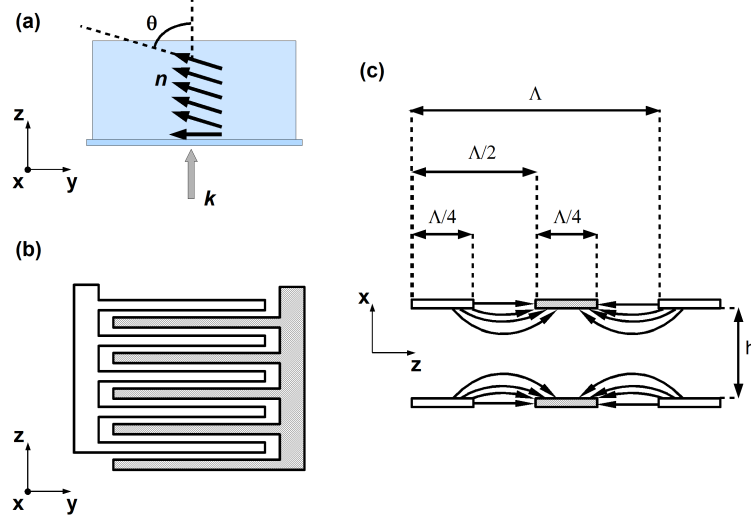
Figure 2.2: Top view of (a) the sample and (b) sketch of the patterned electrodes. (c) Side view of the electrodes with the field lines

a waist variable in propagation, are solutions for such a nonlocal nonlinear system, with period and amplitude of oscillations depending on material parameters and beam power (26). Thus, while in local media the soliton waist is invariant in propagation and completely describes the power dependent behavior, in a nonlocal system *breathing* is the characteristic feature of self-localized waves.

In the cell described above, by varying the applied voltage we are able to change the background angle θ_0 in the bulk nematic: in other words we deal with a system with a tunable nonlinearity. We coupled a beam from an infrared Nd:YAG laser source ($\lambda = 1.064\mu m$), focusing it in $x = 0$ with a waist of about $2.5\mu m$. For every applied voltage (hence for a given nonlinearity) we varied the beam power between 1 and $10mW$, evaluating the beam waist versus propagation: in this way we could control the relationship between the optical torque and the nonlinearity.

Fig. 2.3 shows some of the results. For high background angles, around 80° (i.e. with no voltage or low voltage applied to the cell electrodes), the beam diffracted (except for the highest power), as the optical torque on the NLC molecules is negligible in such a perturbative regime [fig. 2.3(a)]. Lowering θ_0 toward 70°, the nonlinearity became appreciable; self-focusing occurred, with a breathing period progressively reducing from $2mm$ to $600\mu m$ with increasing power, around a mean value comparable with the
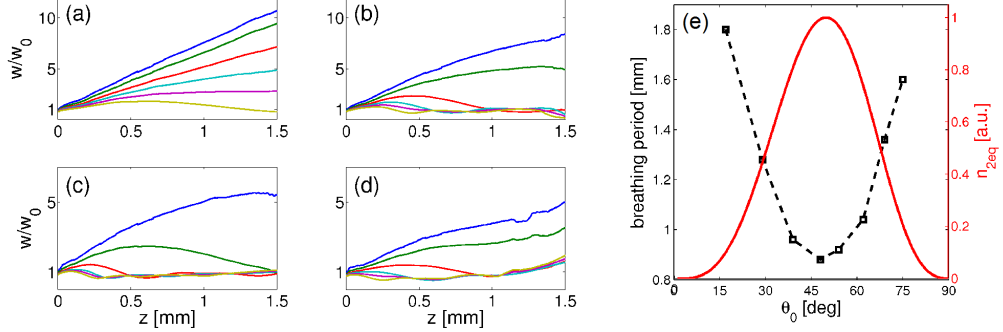
Figure 2.3: Normalized beam waist evolution for θ_0=10(a),20(b),50(c),70(d)$°$, with power varying in the range $P = 1$(blue), 2(green), 4(red), 6(purple), 8(cyan), 10(yellow) mW. (e) The calculated nonlinearity coefficient (red line), from eq. (2.1), and experimental measured breathing period (black squares), for $P = 4mW$, as functions of θ_0

input waist [fig. 2.3(b)]; then, for $\theta_0 \simeq 40°$, self-confinement was enabled (for every power) and the breathing period reached its minimum, $\simeq 120\mu m$ (for $P = 10mW$), demonstrating that the nonlinearity reached the highest possible value [fig. 2.3(c)]. Finally, going towards larger θ_0, the waist oscillations became longer as the nonlinearity was decreasing and at low power diffraction became dominant again [fig. 2.3(d)]. We stress that breathing oscillations were evaluated at the early stage of propagation (typically the first half of the actual period), as scattering losses gradually reduced the beam power, thus preventing the appearance of a purely sinusoidal breathing, as predicted in absence of losses. In the perturbative regime we could compare the observed breathing period with the equivalent nonlinear coefficient of eq. (2.1), both functions of the background angle. Fig. 2.3(e) represents the two curves, the former at $P = 4mW$: as expected, the breathing period decreased from $1.8mm$ to $0.9mm$ for increasing nonlinearity, the minimum period corresponding to the maximum nonlinearity, in $\theta_0 \simeq 45°$.

We can extract extra information from the previous measurements, analyzing the beam trajectory rather than the confinement: as the director $\boldsymbol{n}$ formed smaller and smaller angles with respect to $\boldsymbol{k}$, the birefringent walk-off of the extraordinarily polarized wave propagating in the sample changed according to eq. (1.5), i.e., the Poynting vector $\boldsymbol{s}$ varied its direction with respect to $\boldsymbol{k}$, thereby deviating the corresponding light beam. Fig. 2.4 shows a set of acquired photographs of the beam at $P = 2mW$.
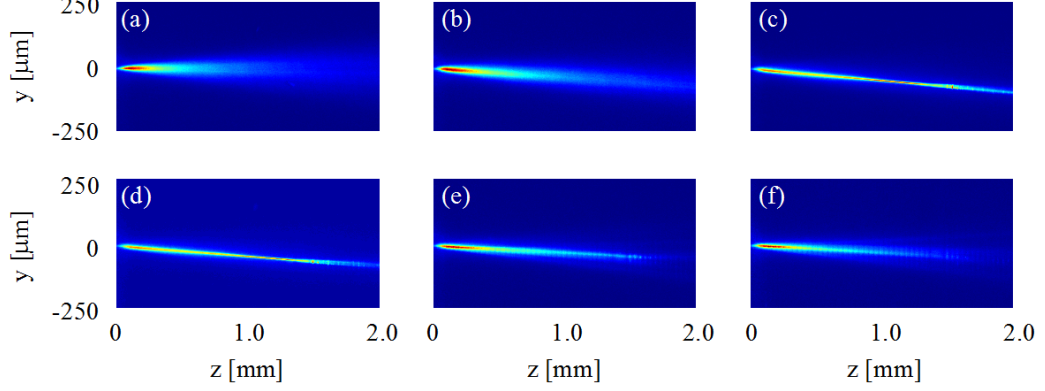
Figure 2.4: Snapshots of beam propagating in the sample for various applied voltages, 0(a), 1.5(b), 2(c), 2.5(d), 3(e), 3.5(f) V, respectively.

For V= $0V$, i.e. for $\theta_0 = 80°$, the diffracting light beam propagated at a corresponding $\delta = \delta(\theta_0) \simeq 2°$. Above V= $1.5V$, the self-focusing became appreciable until a nematicon was generated at V= $1.75V$, with an angle of propagation increased until $\delta(50°) \simeq 6.2°$. A further increase in bias saturated the reorientation and we could observe diffractive propagation together with a smaller walk-off.
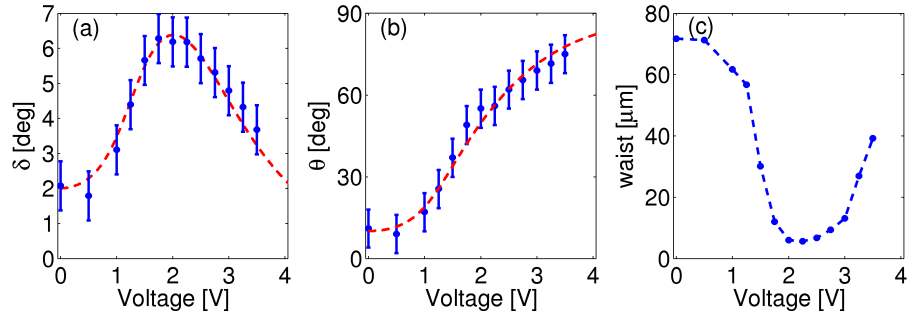
Figure 2.5: (a) Measured walk-off and (b) calculated reorientation angles as functions of the applied voltage. The blue dots are experimental data while the red dashed lines are fits from the model. (c) Beam waist at $z = 1mm$ as a function of the applied voltage. In this case the dashed line is a guide to the eye.

To model this behavior, we can observe that the link between θ_0 and the bias V in the structure described above is equivalent to the action of a single component electric field E_z across a uniform NLC. We can write:

$$K\frac{\partial^2 \theta}{\partial x^2} - \frac{\Delta\epsilon_{RF}}{2}\sin 2\theta \left|E_z\right|^2 = 0 \qquad (2.2)$$

where K is the single elastic constant corresponding to the planar deformation and $\Delta \epsilon_{RF}$ is the dielectric anisotropy. The transverse field inducing reorientation can be cast as $E_z = \alpha(\Lambda)V$, with α a parameter accounting for periodicity and duty cycle of the patterned electrodes, but independent from h. Once found the values for θ_0 from eq. (2.2), the walk-off could be easily calculated by using eq. (1.5). From the observed walk-off versus V and eq. (1.5) we could calculate the electro-optic reorientation angle θ. As plotted in fig. 2.5, the actual response is in perfect agreement with the equivalent structure as modeled by eq. (2.2), with $\theta_0 = \theta_0(\alpha V)$ and $\alpha \approx 0.62$.

2.2 Nonlinearly controlled soliton spiraling

In the previous chapter we discussed how the NLC high nonlocality is due to the influence of the Coulombian intermolecular forces on the director perturbation induced by an optical field. In the highly nonlocal limit, the particular form of the NLSE resembles a quantum harmonic oscillator. (24) With suitable equivalent quantities, such a nonlinear optical system can be studied with the equations used in mechanics.
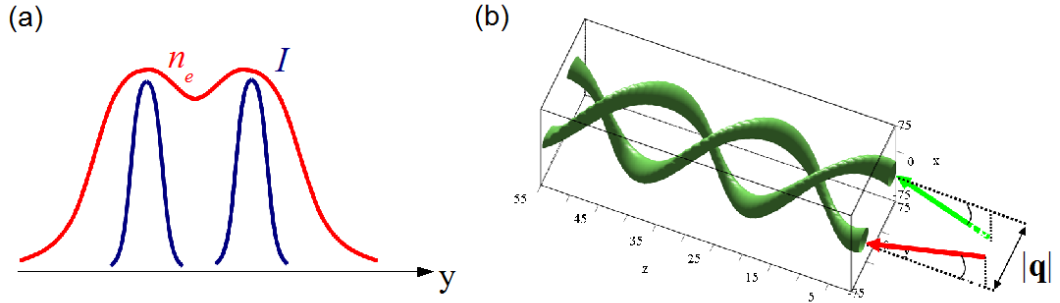
Figure 2.6: Soliton-soliton interactions. (a) Beam profiles (blue) and corresponding index perturbation (red). (b) Sketch of two spiraling solitons.

For two solitons coplanarly propagating in NLC, the resulting index distribution is the sum of the single perturbations: if the separation between the two beams is smaller than the nonlocality range, there will be a zone where the overlap of the two index profiles generates an attractive equivalent force, as in fig. 2.6(a): the two solitons move towards each other depending on their reciprocal distance and the induced index perturbation. Based on the parameters, soliton crossing or merging can be observed. In this framework nonlocality drives soliton interactions. If the solitons are skew, the interaction will occur in a 3D space: the tendency of the beams to follow their initial directions is contrasted by the nonlinear potential. As sketched in fig. 2.6(b), the solitons start to spiral around each other in a double helix configuration.

Soliton-soliton interactions have been studied in several nonlocal media both theoretically (53)(54) and experimentally (55)(56)(28), their control being given by initial conditions, i.e. distance (57), launch angle (58) or phase difference (59). Here we demonstrate a novel approach based on nonlinear control of soliton spiraling, i.e. on power-dependent angular momentum of the soliton cluster.

2.2.1 Model and simulations

Taking the usual form for the soliton solution $A_\alpha = A_0(\mathbf{r}_\alpha)e^{i\phi z}$, where the subscript $\alpha = [1,2]$ indicates one of the two beams and $\mathbf{r} = [x,y]$ is the generic transverse coordinate, then the equivalent soliton *"mass"* can be expressed as its power $m = \int\int d\mathbf{r}^2 \, |A_\alpha|^2$. Considering the two solitons cluster coordinate $\mathbf{q} = [\mathbf{r}_1 - \mathbf{r}_2]$ and generalizing the Ehrenfest theorem (17), we obtain the motion equation:

$$m\frac{\partial^2 \mathbf{q}}{\partial z^2} + \nabla_q U(\mathbf{q}) = 0 \qquad (2.3)$$

where $\nabla_q U(\mathbf{q})$ represents the interaction potential, given by the total index distribution. One conserved quantity in such a system is the total angular momentum $\mathbf{L}$, defined as:

$$\boldsymbol{L} = m\mathbf{q} \times \dot{\mathbf{q}} \qquad (2.4)$$

Eq. (2.4) states that, once defined the initial conditions, the angular momentum is linearly dependent on the mass. In this case it is possible to control the angular momentum by varying the cluster excitation, i.e. the total power $P_{in} = \int\int d\mathbf{r}^2 \, |A_1 + A_2|^2$.
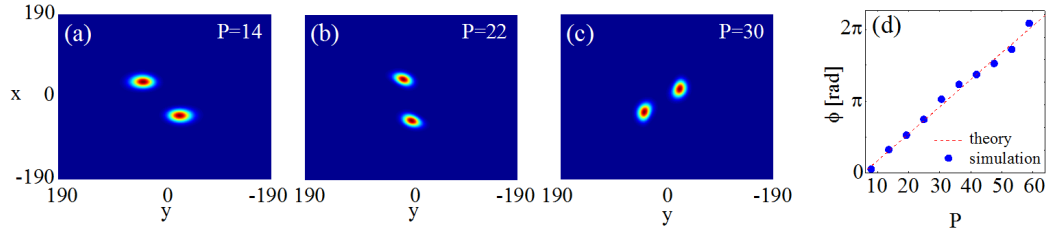
Figure 2.7: Simulations of soliton spiraling: (a)-(c) Output profiles and (d) angular rotation versus initial power, in agreement with theory. The power is expressed in normalized units.

It is worth noting that no hypothesis is made on the medium, so the model holds for every kind of waves propagating in a generic nonlinear nonlocal medium. Simulations for a nonlocal Kerr-like medium are shown in fig. 2.7: the spiraling of two solitons launched with opposite momenta was observed versus power. The angular momentum was represented by the the rotation of the cluster, i.e. the angle $\phi(P)$ described by the solitons evolution with respect to the center of mass of the cluster: as expected, when the power P increased, the equivalent particles rotated [fig.2.7(a)-(d)] with a revolution angle linearly depending on the excitation [fig.2.7(e)], in perfect agreement with theory.

2.2.2 Experiments

We carried out experiments in a planar cell with a $100\mu m$ thick layer of liquid crystals E7 planarly anchored at $\theta_0 = \pi/6$, using a near-infrared ($\lambda = 1.064\mu m$) cw source. Two high-resolution CCDs were used for imaging both the solitons propagation in the yz plane and their output position or transverse profile in the xy plane. We excited two nematicons by launching two extraordinary-wave gaussian beams slightly tilted to give them opposite momenta, taking care that no interactions with boundaries occurred at any power. Our experimental results are summarized in fig. 2.8: images of nematicon propagation [figs. 2.8(a)-(d)] and the corresponding output intensity profiles [figs. 2.8(e)-(h)] for increasing power are illustrated. In agreement with both analytical and numerical predictions, as the power changed from 2.1 [figs. 2.8(a),(e)] to $3.9mW$ [figs. 2.8(d),(h)], the angular momentum of the soliton cluster changed as well, as demonstrated by the 180° rotation in the output plane. It must be stressed that each soliton profile evolved nearly unmodified. Finally, fig. 2.8(i) shows the rotation of the soliton cluster: the angle is linear with total power, in perfect agreement with theory.
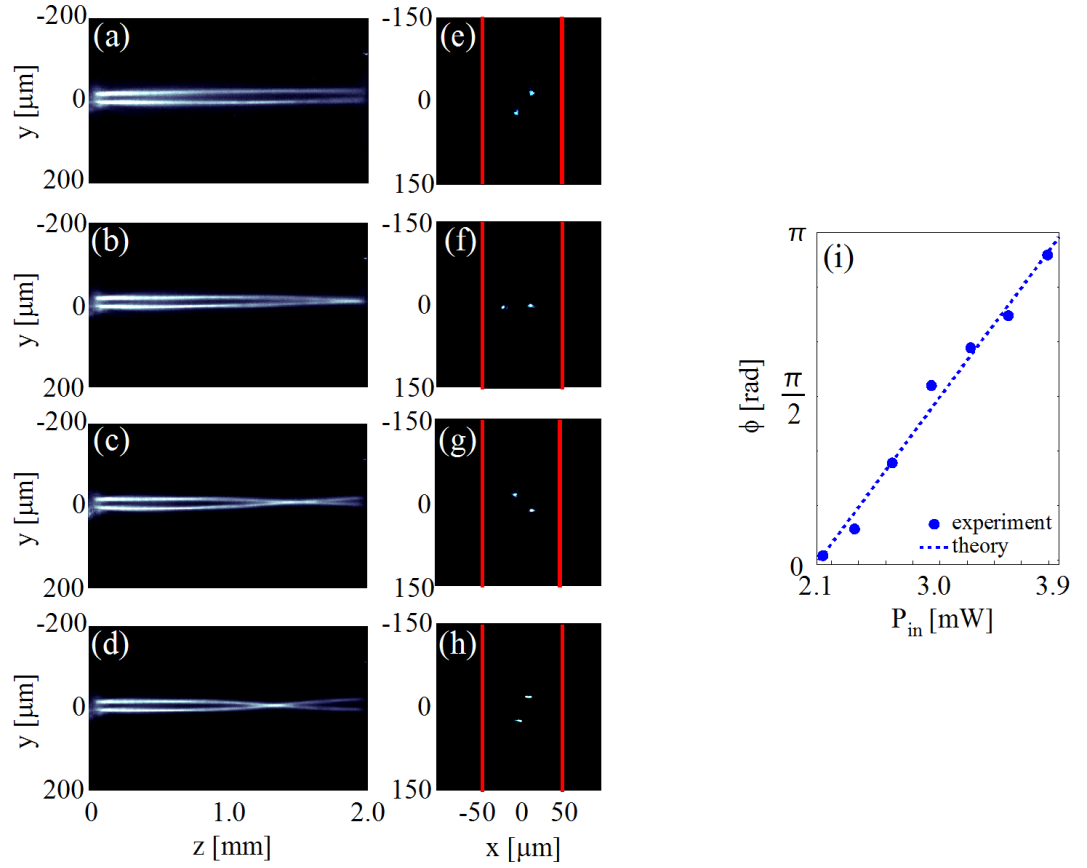
Figure 2.8: Experimental results on soliton spiraling: (a)-(d) propagation and (e)-(f) output profiles for various initial powers. At P_{in}=2.1mW (a),(e) the two beams propagate slightly tilted. Increasing P_{in}, the two beams rotate around their center of mass until, for P_{in}=3.9mW (d),(h), a rotation of π is obtained. (i) Rotation angle versus initial power. Owing to the huge nonlinear response of NLC, the rotation rate is $\Delta\phi/\Delta P = 0.5 rad/mW$.

2.3 Conclusions

In this chapter we disclosed a few nematicon properties related to the nonlocal nonlinear nature of NLC and discussed some experimental results supported by theoretical models. In the first part we proposed a novel cell geometry in which it is possible to tune the NLC nonlinearity as well as the nematicon trajectory with an electric control. In the reported experiments, by affecting the initial conditions we observed diffractive, confined and breathing regimes, as well as in-plane beam steering. The second part was dedicated to nonlocality mediated soliton-soliton skew interactions. Both simulation and experiments confirmed the results of the model: the angular momentum associated to a cluster of two (or more) solitons can be nonlinearly controlled simply acting on the system excitation.

Besides their interest for the understanding of soliton properties, these two examples can easily turned into simple devices for applications in optical signal readdressing and processing. In the sample with the patterned electrodes, as the induced waveguides change their guidance when the background angles varies, a mode selector can be realized; a voltage-controlled signal demultiplexer can be easily implemented by assigning a position to every value of the applied field. Finally, by exploiting soliton spiraling, a 3D nonlinearly controlled signal router can be implemented in which the output ports depend on the total power.

3

Dye-doped nematic liquid crystals

In the early nineties a paper by Janossy and co-workers (60) reported some experiments on Dye-Doped Nematic Liquid Crystals (DDNLC): they found that the Freedericksz's threshold in an NLC, in which small quantities (less than 1%) of an anthraquinone derivative (61) had been dissolved, was remarkably lower than in undoped NLC, even if the other optical and mechanical properties remained unaltered. (62) Later studies were conducted by varying concentration, guest-host system and excitation wavelength, leading to models of the effect of a dye as an equivalent additional torque τ_{dye} acting on the molecular system (63)(64):

$$\tau_{tot} = \tau_{NLC} + \tau_{dye} \tag{3.1}$$

This effect is known as the *Janossy effect*. Depending on the parameters, the amplitude of τ_{dye} can vary considerably, so that it can become comparable to τ_{NLC} or higher. The sign of τ_{dye} can change too, reducing the total torque or even changing its sign, with an equivalent optical self-defocusing response of the mixture. (65)(66)(67) A phenomenological model was developed, based on the interaction energy of the guest-host (NLC-dye) system. The dye molecules in the ground state are bound to the NLC matrix; the radiation absorbed by host molecules drives their transition to one (or more) excited state(s), thus changing the interaction potential with the guest and eventually affecting the director distribution. (67)(68) Hence, the equivalent optically-induced effect is due to a dye-mediated interaction between the optical field and the NLC.

Despite the studies of DDNLC (69)(70)(71) a unified theoretical model is still lacking, as it depends on the peculiar guest-host interaction during and after the transition of the dye to an excited state. (67)(68) Reported experiments on DDNLC cover a large range of phenomena, from the simple optically-induced heating (72), to molecular conformational changes (73) and to interactions with surfaces. (65)(74) Spatial solitons in DDNLC were investigated in samples where a combined action of orientational and thermal nonlinearities took place. (75) The interactions with "defects" in the molecular order, generated by external beam via *azo*-dyes *Trans-Cis* transitions, were employed to implement logic functions. (47)

In this chapter we describe two experiments conducted in DDNLC. In the first we show the self-action of light and the fundamental differences between undoped and doped NLC. In the second we employ another dye-induced effect to generate optical interfaces affecting the nematicon trajectory.

3.1 Self-Steering of nematicons

Eq. 1.8 predicts power dependent walk-off, as the torque exerted on the NLC molecules changes the angle θ and, eventually, $\delta(\theta)$. Soliton steering due to self-action is ruled by the Ehrenfest theorem, deriving the equivalent transverse force acting on the beam:

$$\mathbf{F}(z) = \left[\left(n_e \frac{\partial n_e}{\partial x} \right) \hat{x} + \left(n_e \frac{\partial n_e}{\partial y} \right) \hat{y} + \left(1 + \tan^2 \delta \right) \frac{\partial \delta}{\partial z} \hat{y} \right] \Bigg|_{x=x_b, y=y_b} \tag{3.2}$$

evaluated in $\boldsymbol{r}_b = \int \int \boldsymbol{r} \, |A|^2 \, dxdy / \int \int |A|^2 \, dxdy$ with $\mathbf{r} = [x, y]$, i.e. at the soliton center of mass. If the beam is launched in $x = h/2$, the first two terms are null and the only force is due to the presence of walk-off.

Nonlinear walk-off in NLC was previously reported analyzing patterns in modulation instability at large power; for power ensuring soliton stability at typical values of θ_0 ($\pi/6 < \theta_0 < \pi/3$), optical reorientation is of the order of few degrees, thus the nonlinear walk-off variations are negligible. Higher powers generate transverse instabilities and the soliton position is not measurable due to lateral fluctuations. To design a suitable cell in which to observe nonlinear self-steering, we analyzed eq. 1.5 and its derivative:

$$\frac{\partial \delta}{\partial \theta_0} = \frac{1 + 2\Phi_\epsilon \cos 2\theta_0 + \cos^2 \theta_0}{1 + 2\Phi_\epsilon \cos 2\theta_0 + \Phi_\epsilon^2} \tag{3.3}$$
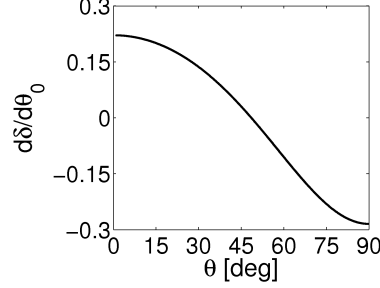
Figure 3.1: Walk-off δ derivative with respect to θ_0: it is null when nonlinearity is maximized ($\theta_0 \approx 45°$), while it reaches the highest values towards $\theta = 0$ or $90°$.

with $\Phi_\epsilon = 1 + 2\epsilon_\perp/\epsilon_a$. Maximizing the nonlinearity (i.e. for $\theta_0 \approx \pi/4$), large variations of θ, corresponding to high intensity, are needed to obtain appreciable walk-off variations [figs. 1.2(b) and 3.1]; in this regime instabilities prevent any measurements of nonlinear self-steering. For angles approaching $\theta_0 \approx 0$ or $\theta_0 \approx \pi/2$, $\partial\delta/\partial\theta_0$ is much larger (fig. 3.1) and nonlinear walk-off changes require lower intensities. A suitable trade-off between the change in walk-off and the nonlinear reorientation is $\theta_0 = 4\pi/9$. In a cell prepared with this angle, we found that a near-infrared laser ($\lambda = 1064nm$) focused to a waist $w_0 = 3\mu m$ could excite solitons up to $60mW$ without instabilities.
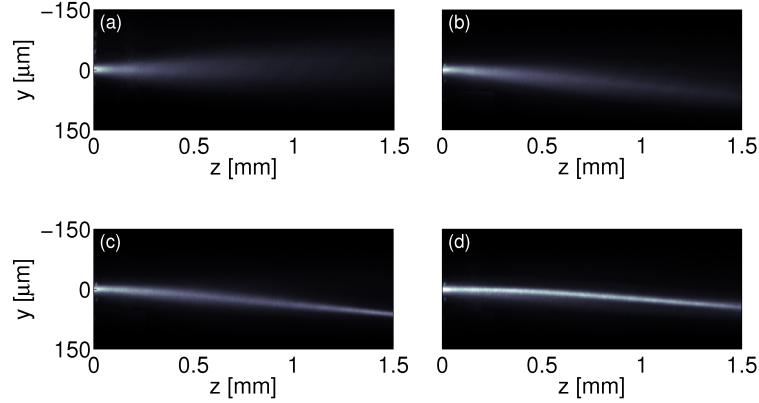
Figure 3.2: Nematicon self-steering. (a) Ordinary component. (b) Diffracting extraordinary component, for $P = 10mW$. Self-confinement occurs at (c) $P = 20mW$ and the high reorientation steers the solitons reducing the walk-off until (d) $P = 60mW$, when instabilities begin to be observed.

As shown in fig. 3.3, the threshold for soliton formation in this cell is much higher than for $\theta = 45°$ owing to the lower nonlinearity; the extraordinary-wave beams started
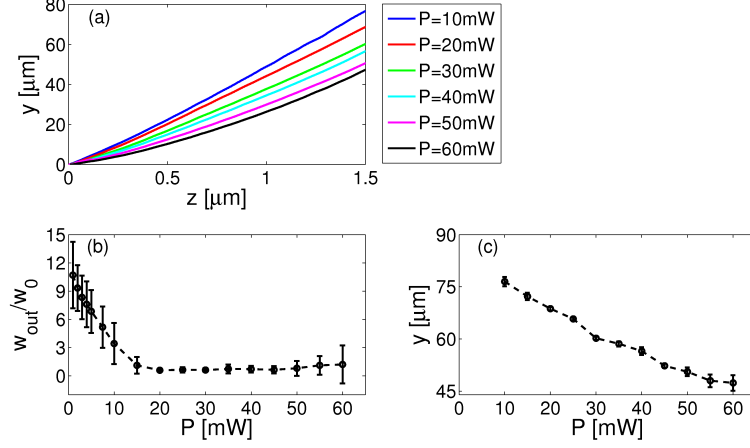
Figure 3.3: (a) Calculated soliton trajectories for various input powers: the z-dependence of the trajectory depends on a decreasing optical reorientation due to scattering losses. (b) Normalized beam waist versus input power at $z = 1mm$: the nonlinearity at $\theta_0 = 80°$ is lower than for $\theta_0 = 45°$ and self-focusing is observed for higher powers. The different error bars depend on the beam size comparable with the cell thickness at low powers and on lateral fluctuations at high powers. (c) Soliton deflection in $z = 1.5mm$: for $P \leq 10mW$ the beam center cannot be evaluated correctly, as the beam is as large as the cell.

to experience self-focusing around $P = 10mW$, eventually reaching a self-trapped regime at $18mW$, as can be appreciated from the waist measurement in fig. 3.3(b). Between 1 and $60mW$ molecular reorientation led to relevant changes in walk-off (see fig. 3.2). Due to scattering losses (measured $\alpha \simeq 6cm^{-1}$), we observed a z-dependent behavior [fig. 3.3(a)] as intensity decreased in propagation and optical reorientation, too: as a result, the soliton trajectories were curved, but nearly parallel for $z >> \alpha^{-1}$. The final deflection calculated at $z = 1.5mm$ and for $P = 60mW$ is $\Delta y \approx 30\mu m$ [fig. 3.3(c)], corresponding to a maximum local deflection angle of $\approx 2°$.

Though the experiments demonstrated self-steering in undoped NLC, the angular deviation was limited by instabilities at high powers. As the problem rests on the value of nonlinearity, DDNLC can be a route towards enhancing the maximum obtainable steering.

3.1.1 Self-Steering in DDNLC

As pointed out above, the presence of a dye changes the reorientational response of the NLC: for a more efficient self-steering we need a dye which increases the optical

torque. We employed a planar cell with a thickness $L = 75\mu m$ and $\theta_0 = 45°$ filled with a mixture of E7 and 1-Amino-Anthraquinone (1-AAQ) in a weight ratio of 100:1, with an absorption peak around $0.5\mu m$; treatment at the input interface anchored the NLC molecules at an angle $\theta_{in} = 90°$, corresponding to the director along y. In this case the angular distribution at the center of the cell can be obtained from the reorientation equation in the absence of excitation, i.e. $\tilde{\theta} \approx \theta_0 + (\theta_{in} - \theta_0)\,e^{-z/L}$. To excite the dye mediated response, we used a He-Cd Laser at $\lambda = 442nm$, for a compromise between magnitude of the Janossy effect and tolerable beam attenuation. Nonlinear propagation in such media is still described by eq. (1.8), while eq. (1.9) becomes:

$$\nabla^2\theta + \gamma(1+\eta)\{(|E_t|^2 - |E_s|^2)\sin[2(\theta - \delta)] + 2\Re(E_t E_s^*)\cos[2(\theta - \delta)]\} = 0 \qquad (3.4)$$

where η is a coefficient accounting for the Janossy effect (it gives an equivalent gain in molecular torque); E_t and E_s are the transverse and longitudinal electric field components, respectively, in a z-dependent reference system xts obtained from xyz after rotation by δ around x, such that s is collinear to the point-wise Poynting vector. We expect self-confinement to occur at low power: as illustrated in fig. 3.4, due to dye dichroism, the Freederickz's threshold prevented reorientation for ordinary waves, while self-focusing occurred for extraordinary polarization just above $100\mu W$ and a solitary wave was observed for $P = 160\mu W$. The latter propagated at a walk-off angle $\delta \approx 9°$, as the refractive indices are $n_{||} = 1.8129$ and $n_{\perp} = 1.5426$ for $\lambda = 442nm$. Measured absorption gave $\alpha \approx 50cm^{-1}$; hence, after a few hundreds microns the reduced intensity brought back the beam to propagate in the linear regime. A first remarkable result was the experimental demonstration of dissipative solitons at $sub\text{-}mW$ powers.

From eqs. (1.8)-(3.4) one would expect beam self-steering similar to that observed in undoped NLC, although for lower intensities: as the soliton profile and the non-linearly induced index well are evenly symmetric in the transverse coordinate t, the soliton wavevector remains constant versus propagation and steering is only caused by changes in walk-off (76): naming ϕ the angle between s and z, it is $\phi = \delta$, i.e. the soliton trajectory corresponds to what predicted for plane-waves.

Fig. 3.5(a)-(c) summarizes the expected beam evolution in DDNLC: after the non-homogeneous transition region by the input interface ($z = 0$), a low-power beam diffracts as it propagates along its (linear) Poynting vector s with walk-off $\tilde{\delta} = \delta\left(\tilde{\theta}\right)$
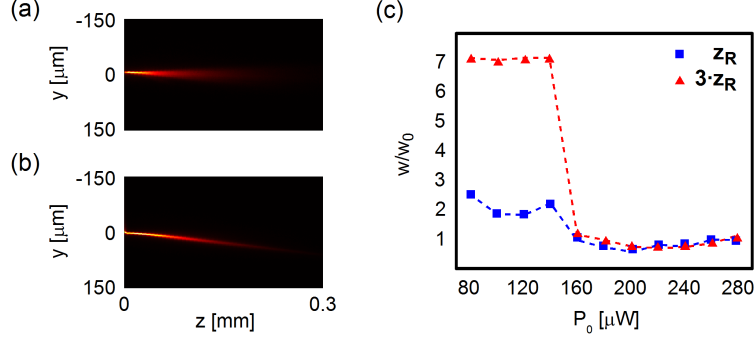
Figure 3.4: (a) Ordinary and (b) extraordinary wave propagation for an excitation $P_0 = 160\mu W$. The extraordinary component propagates with $\phi(z) = \tilde{\delta}(z)$.

with respect to $\boldsymbol{k}$ [fig. 3.5(a)]; at higher power [fig. 3.5(b)] self-focusing and self-confinement take place via reorientation, balancing out diffraction and yielding a solitary wave; when [fig. 3.5(c)] reorientation becomes comparable with $\tilde{\theta}$, it affects the beam trajectory by reducing the walk-off. In all cases (in analogy to undoped NLC), owing to scattering and absorption which exponentially reduce the power and therefore the nonlinear perturbation in θ, the soliton eventually travels with its initial wavevector and walk-off $\delta_0 = \delta(\theta_0)$, irrespective of the excitation.

Fig. 3.6(a)-(h) displays photos of beam evolution in yz for increasing excitation P_0. At low power and beyond the initial transition region, the e-polarized beam propagated at an angle $\delta_0 \approx 9°$ with z, as expected for plane waves (rays) at $\lambda = 442nm$ (fig. 3.6(a)). As P_0 increased from 80 to 160 [fig. 3.6(b)], 180 [fig. 3.6(c)] and $220\mu W$ [fig. 3.6(d)], respectively, light induced reorientation gave rise to filament self-steering as the walk-off progressively reduced to nearly zero and $\boldsymbol{s}$ tent to align with z.

From a careful observation of the beam trajectories, it can be noted that they remained straight for large z: nonlinear walk-off cannot explain this behavior in such a dissipative medium. This counterintuitive behavior corresponds to a rotation of the wavevector $\boldsymbol{k}$. Above $P_0 = 260\mu W$ [fig. 3.6(e)-(h)], a diffracting ordinary-wave appeared, while the extraordinary confined wave steered to negative angles, reaching $\phi \approx -30°$ for $P_0 = 400\mu W$ [fig. 3.6(h), as in fig. 3.5(d)]. Therefore, in the range $160 - 400\mu W$, self-steering over $\approx 39°$ was observed for the self-guided e-beam, with an additional ordinary component revealing a tilt of the optic axis $\boldsymbol{n}$ out of the plane yz.

Eq. (3.4) needs to be modified to correctly describe the observed behavior. From
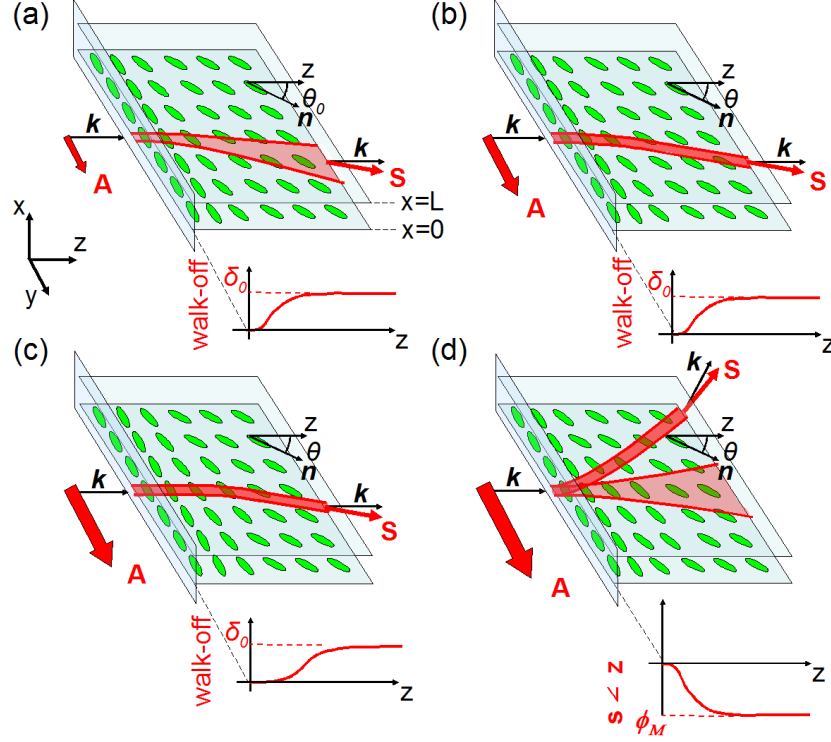
Figure 3.5: Sketch of the cell and nonlinear beam propagation in NLC doped with 1-AAQ. (a)-(c) Light beam evolution based on a plane-wave model. The 2D graphs show walk-off versus propagation in three cases. (a) Beam propagation in the linear (diffractive) regime. (b) Self-confinement: the excitation generates a soliton with unaltered walk-off $\delta = \tilde{\delta}$. (c) Nonlinear change in walk-off. (d) Pictorial rendering of the obtained experimental results at higher excitations: the soliton gets steered towards negative y (4th quadrant in the plane yz), with the appearance of an ordinary component propagating along z.

the experimental trajectories, it can be appreciated that steering towards negative y already occurred near the input interface. Since the steering depends on power, the phenomenon must have a nonlinear origin. Moreover, having verified that absorption-induced thermal effects were small and produced negligible beam deviations, the change of wavevector $\boldsymbol{k}$ can be explained only by an odd asymmetry in the index profile; despite the large birefringence, power-dependent walk-off cannot introduce such an asymmetry to explain the observed large soliton steering. As nematicons are expected to narrow-down to wavelength size, the transverse asymmetry can be associated to the longitudinal field component E_s, exhibiting an odd profile if the transverse field E_t is even. To account for the odd symmetry of E_s we took a Janossy coefficient
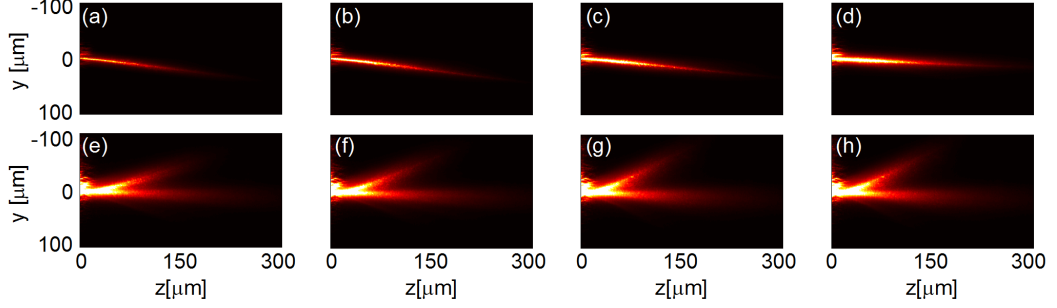
Figure 3.6: Evolution of an extraordinarily polarized beam in yz for various excitations P_0. (a)-(d) Input powers are $80 - 160 - 180 - 220\mu W$, respectively, with Poynting vector spanning angles from $9°$ to $0°$ at large z. (e)-(h) Input powers are $260 - 300 - 340 - 400\mu W$, respectively, with negative angles and the appearance of an ordinary component diffracting along z. The beams appear wider than they are as the images result from collection of scattered light.

$\eta = \eta_I/(1 + I/I_{sat}) + \Delta\eta$, with $\Delta\eta = c\Im(E_s e^{-i\beta z})$, β the soliton propagation constant, c an intensity-dependent phenomenological coefficient and I the light intensity. We considered a saturating response to account for the high intensities involved due to the strong confinement. Considering the reorientation angle θ as the sum of a term ϕ due to the purely optical reorientation and of a term $\Delta\phi$ due to the index asymmetry, eq. (3.4) becomes:

$$\nabla^2_{xy}\Delta\phi + \alpha^2\Delta\phi = -\Delta\eta \sin\left[2(\theta_{max} - \delta(\theta_{max}))\right] |E_t|^2 e^{\alpha z} \tag{3.5}$$

where the subscript ''max'' refers to the maximum value for a fixed z and where we considered $\Delta\phi << \phi$ and $E_s << E_t$. Applying the Ehrenfest theorem we obtain the soliton trajectory under the action of an equivalent transverse force F_{tr}:

$$F_{tr} = \chi e^{-\alpha z} P^{3/2} w^{-2} \tag{3.6}$$

$$\frac{d^2 y_m}{dz^2} = \frac{d \tan\delta}{dz} + F_{tr}(w, P) \tag{3.7}$$

where y_m is the soliton position (taken on the beam axis), χ depends on optical reorientation and $P = P_0 e^{-\alpha z}$.

A comparison between measured and calculated trajectories, in fig. 3.7(a)-(b), together with the curve describing the solitary wave deflection as a function of input
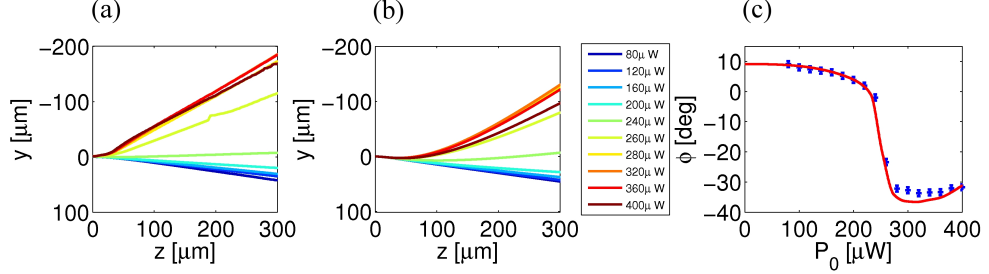
Figure 3.7: (a) Experimental and (b) simulated trajectories for P_0 varying from 80 to $400\mu W$. (c) Angular deflection versus initial power. The blue dots are experimental values while the red line is derived from eq. (3.7) ($I_{sat} = 0.5mW/\mu m^2$ and $\eta_I = 50$).

power [fig. 3.7(c)], show the good agreement between the model and the data. The trend in ϕ [fig. 3.7(c)] resembles the optical Freedericksz transition; hence, $\Delta\eta$ can be associated to reorientation of the optic axis out of the plane yz, mediated by the anisotropy inherent to the guest-host interaction in dye-doped NLC and in perfect agreement with the appearance of the ordinary-wave component at high powers (fig. 3.6). At low powers the system is below the Freedericksz threshold and within the Mauguin limit (33); above threshold, changes in $\boldsymbol{n}$ near the input interface are no longer adiabatic and coupling occurs between ordinary and extraordinary field components. In the transition region at the input, in fact, the optic axis distribution varies on a scale smaller than the minimum cell dimension (thickness L), ensuring a nonlocal range $< L$.

3.1.1.1   Dye luminescence in NLC

Since 1-AAQ is optically active, the absorption of blue photons (442nm) is associated to the population of an excited state with subsequent radiative emission of red light via photoluminescence. (77) We separated blue and red components by the use of a band-pass filter (centered around $633nm$) and acquired images of the spontaneously emitted photons excited by blue beam(s), as visible in fig. 3.8. It is clear that the emitted red photons diffracted (ordinary wave, fig. 3.8) or got confined (extraordinary wave, fig. 3.8) depending on the polarization of the blue waves, i.e. they retained the input polarization and Poynting vector. Although the two different wavelengths are associated to different walk-offs (namely $\delta_{442nm} \approx 9°$ and $\delta_{633nm} \approx 6°$) due to the NLC dispersion [see eq. (1.5)], in the confined case the red light was efficiently trapped by
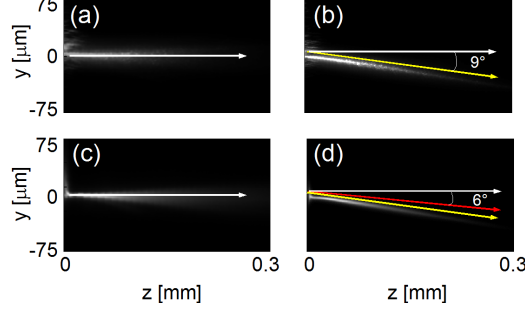
Figure 3.8: Comparison of beam evolution of blue and corresponding red emitted light. (a) and (c) correspond to ordinary polarization, while (b) and (d) are extraordinary self-confined waves. White lines are directed along the wavevector $\boldsymbol{k}$, while yellow and red lines correspond to the direction of the Poynting vector for plane waves at 442 and $633nm$, respectively. Noteworthy, the trapping overcomes the natural walk-off of the red light.

the nematicon waveguide owing to reorientation. Such confinement took place despite the longer wavelength, thanks to the large numerical aperture of the nematicon as stemming from the highly nonlocal response of the NLC. The emitted probe travelled along the nematicon trajectory, undergoing attenuation and walk-off consistently with the evolution of the blue soliton (fig. 3.8).
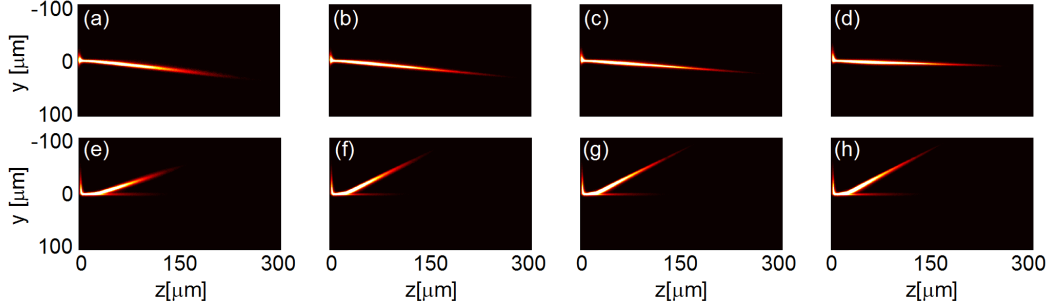
Figure 3.9: Evolution of the red light generated by dye photoluminescence and trapped in the soliton-induced waveguide. In (a) through (h) the corresponding input powers at $\lambda_{blue} = 442nm$ are those indicated in fig. 3.6. Since $(\lambda_{red})^2 >> (\lambda_{blue})^2$, Rayleigh scattering $(\propto \lambda^{-2})$ in NLC) is much lower than at λ_{blue} (see fig. 3.6).

Finally, fig. 3.9 shows the images acquired with the use of the red filter, corresponding to those of fig. 3.6. Noteworthy, owing to Rayleigh scattering, which in NLC is proportional to the squared inverse of the wavelength (33), the acquired images of the (guided) red component appear sharper than those of the blue nematicon.

3.2 All-optical interfaces

As nematicons demonstrate robustness against non uniform director distributions, it is interesting to analyze their behavior when interacting with finite-size inhomogeneities in the molecular alignment. In terms of all-optical signal processing, the use of external light beams locally altering the director distribution seems a suitable choice towards reconfigurable systems. Previous works reported studies of soliton deflections both in doped (47) and undoped (46) NLC. Hereafter, with the use of a DDNLC, we demonstrate refraction and reflection of nematicons at optical interfaces.

3.2.1 Set-up description

We used the 5CB liquid crystal, with a small quantity (0.1% in weight) of Methyl-Red (MR) in a $75\mu m$ thick cell. The input interface maximized the input coupling of light into the extraordinary polarization along y; only one of the interfaces defining the cell was treated, ensuring planar anchoring at $\theta_0 = \pi/4$.
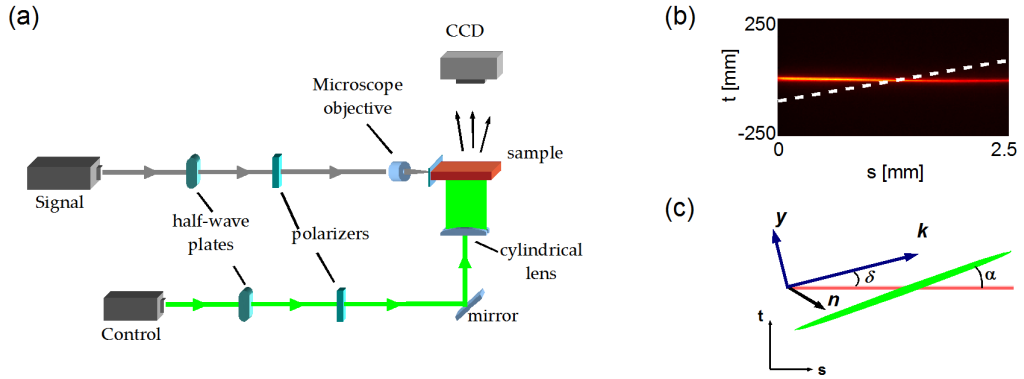
Figure 3.10: (a) Experimental set-up: the control beam impinges transversely to the signal beam (nematicon) and modifies the director distribution. (b) Photo of the nematicon in the reference system of the Poynting vector (direction $\boldsymbol{s}$) with no control beam. White dashed line is the position of the elongated control beam. (c) Sketch of the arrangement of signal and control beams.

An external beam at $\lambda = 532nm$ impinged on the untreated interface of the cell and interacted with the MR molecules, as sketched in fig. 3.10. (78) The green light is known to modifies the interaction energy between MR and the surface, causing

their *absorption/desorption.* (74) Due to the dye dichroism, the polarization-dependent balance between adsorption and desorption determines a preferred orientation of the dye molecules, which can be controlled by intensity, exposure time, and wavelength. (74)(79) This orientation provides anchoring-like conditions for the DDNLC, inducing a preferred director orientation at the surface and, through elastic forces, in the whole thickness of the cell, thereby allowing a complete external control of the optical properties of the bulk medium below the illuminated region. In particular, for the moderate intensities we used in the experiments, the DDNLC director tends to reorient perpendicularly to the field polarization. The beam at $532nm$, hereafter named *control beam* (subscript "c") was tailored to a strongly elongated elliptic shape. Another beam at $\lambda = 1064nm$, or *signal beam* (subscript "s"), generated a nematicon of waist of $\approx 5\mu m$ with a wavevector $\mathbf{k}\|z$. The angle between the Poynting vector of the signal beam and the long axis of the control beam was $\approx 9°$.
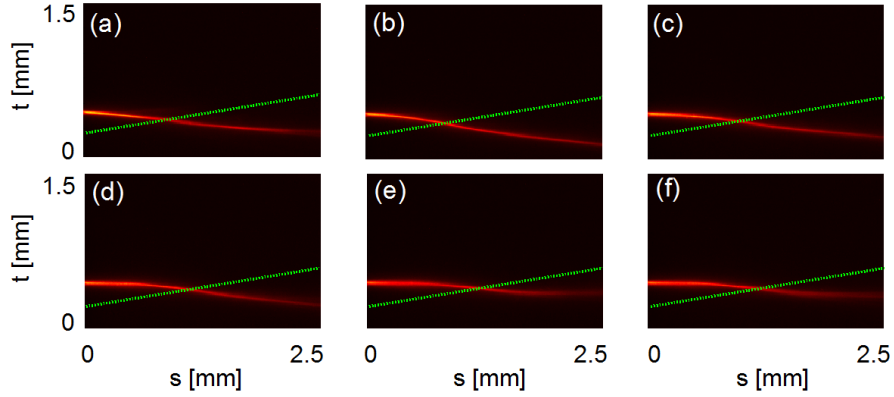
Figure 3.11: Evolution of the signal beam interacting with a defect induced by light polarized along z: the increase in refractive index causes double refraction, with a power dependent soliton deviation. (a) to (f) correspond to $P_c =$[1 6]mW

In this geometry, the surface mediated all-optical reorientation was able to lower/increase the refractive index perceived by the soliton depending on the polarization of the control beam (linear along y/z). Thereby a potential barrier/dip was defined for the nematicon traveling across such graded index region. The effective width and shape of the perturbed region was due to the combined effects of the gaussian profile of the control beam, the nonlocal response of the NLC, the saturating response of DDNLC (due to
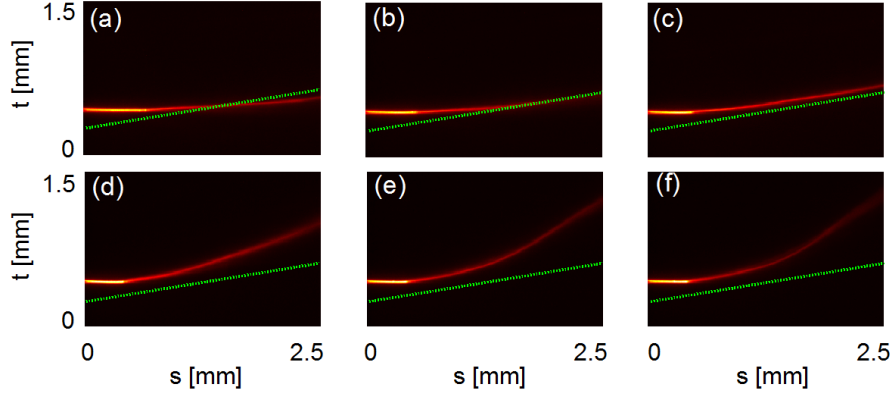
Figure 3.12: Evolution of the signal beam when the control beam decreases the refractive index. When the difference of index is low the soliton passes through the interface, as in (a) and (b) for $P_c = 1$ and $2mW$, respectively. At (c) $P_c = 3mW$ the nematicon remains by the surface, while for (d),(e),(f), corresponding to $P_c = 4, 5, 6mW$ respectively, it undergoes total internal reflection.

the finite dye concentration) and the varying walk-off along the soliton path. When the soliton approached the boundary of this graded index perturbation, it could either travel through it undergoing refraction (twice) or got repelled owing to total internal reflection. At low intensities, the optical reorientation induced by the control beam was negligible, both in magnitude and sign, with respect to the dye surface-mediated effect. We fixed the power of the signal $P_s = 1.5mW$ and varied the control beam intensity from 1 to $6mW$, for polarizations parallel and perpendicular to $\boldsymbol{k}$. For E_c parallel to z, the surface-mediated reorientation produced an increase in the refractive index, creating two graded interfaces where the incoming solitons underwent double refraction, as visible in fig. 3.11.

For E_c parallel to y, the dye-induced reorientation produced a decrease in the extraordinary refractive index, i.e., an optically rarer region. As apparent in fig. 3.12, for control powers $P_c \approx 3mW$ the nematicon became nearly tangential to the interface. We could calculate a critical angle close to $81°$ and an index decrease of ≈ 0.05, with an estimated surface-mediated reorientation of about $13°$. At higher control powers the soliton bounced off the first interface, undergoing total internal reflection. Fig. 3.13 shows the soliton displacement following the interaction with the dye-induced perturbation in the two polarization. The non-monotonic trend in refraction, as pointed
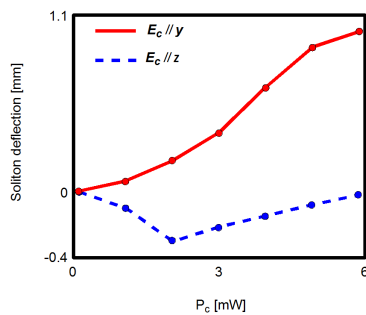
Figure 3.13: Nematicon deviation at $z = 2.5mm$ for control beam generating a potential dip (blue) and barrier (red).

out above, was due to the complex interplay of anisotropy, walk-off, nonlocality, shape of the perturbation and soliton profile. The growing displacement under reflection is associated with an increasing lateral shift of the soliton as the refractive index decreases.

3.3 Conclusions

We illustrated a few experiments with DDNLC, exploiting dyes interactions with NLC molecules. We first reported on the self-action of light on its own trajectory, comparing undoped and doped NLC. In the former case, large nonlinear reorientation induced power dependent walk-off; in the latter case, 1-AAQ enhanced the nonlinear response, with the appearance of a non-negligible longitudinal field of odd parity and thus a transverse force acting on the solitary waves. Then we investigated the interaction of nematicons in a linear index distribution modified by surface-mediated reorientation due to MR adsorption/desorptions.

Again, the two examples disclosed the possibility of implementing routing strategies: self-steering can be employed for nonlinearly controlled signal routing, while the use of external beams in MR-doped cells can control nematicon-based signal re-addressing systems.

4

Nematicons in Liquid Crystal Light Valves

In this chapter we present a novel environment for nematicon all-optical control, based on light induced modulation of director distribution in the Liquid Crystal Light Valve (LCLV). The first section is a brief introduction on the LCLV as a suitable device to control the NLC nonlinearity; the next section is an overview of the valve characterization in terms of nematicon electrical/optical response; the theoretical approach is then described, together with experimental results. Finally, some examples of both digital and analogic all-optical signal processing schemes are presented.

4.1 The Liquid Crystal Light Valve

In 1970 Van Raalte proposed a devise for image projection: he employed an electron beam to modulate the mechanical response of a metal thin film, thus regulating the light brightness on a screen. He called this device *Light Valve.* (80) The same idea was developed by Margerum in an NLC sample: in a biased NLC cell, photo-induced charges on a photoconductive layer modified the transmission of the NLC layer placed between polarizers. It was the first example of an LCLV. (81) During the last five decades LCLV have become an established paradigm in nonlinear optics, as they grant access to a large number of phenomena. Using the valve in transmission or with optical feedback (82) many fundamental effects have been observed, including chaos (83), localized light structures (84), two-wave mixing (85), slow light (86).
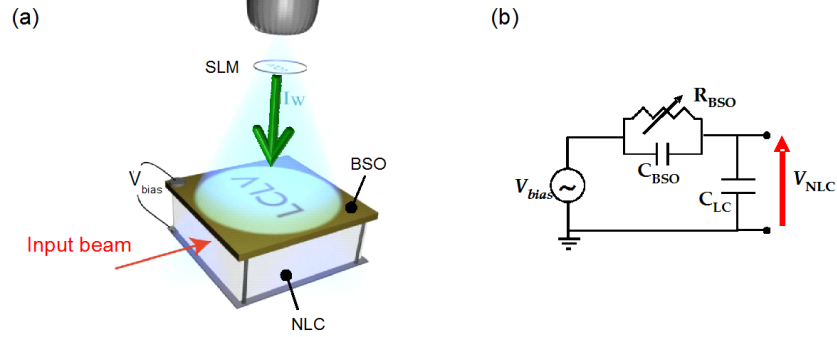
Figure 4.1: (a) Sketch of the LCLV: the $532nm$ $beam$ is tailored by the spatial light modulator (SLM) to a spot of controlled size and shape on the BSO layer. The altered director distribution affects the soliton trajectory. (b) LCLV equivalent electric circuit

With reference to fig.4.1, we used an LCLV similar to a standard planar NLC cell, with one of the interfaces in a photoconductive material, namely Bismuth Silicate (BSO). (87)(88) The cell thickness was $50\mu m$ and we filled it with the nematic E48 ($\Delta n = n_e - n_o \approx 0.23$). Applying a low frequency voltage V_{bias} between the ITO deposited on the glass slide and the BSO, the latter acts like a variable resistor (87): the voltage drop on the NLC layer (V_{NLC}) is given by the voltage divider corresponding to the impedance-ratio of NLC and photoconductor [fig. 4.1(b)]. When radiation of suitable wavelength impinges on the BSO layer, the photogenerated charges modify the photoconductor resistance as well as the voltage drop on the NLC: a point-dependent voltage $V_{NLC}(x, y, z)$ is established, with magnitude and shape defined by the beam (hereafter called *control beam*) intensity and profile, respectively.

A good linear approximation for V_{NLC} is given by (82):

$$V_{NLC} = \gamma V_{bias} + \alpha I(y, z) \tag{4.1}$$

where *I(y,z)* is the beam shape, γ and α are two parameters; the former is derived from the voltage divider, thus depending on liquid crystal and BSO dielectric constants (89), voltage frequency and cell thickness; the latter accounts for the photoconductor optical response.
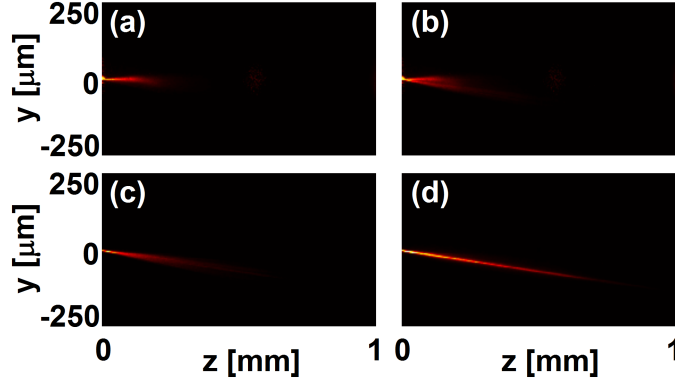
Figure 4.2: Images of the beam propagation in the unbiased LCLV. (a) Ordinary, (b) mixed and (c)-(d) extraordinary polarization. In (d) the high power enables beam self-confinement

4.2   Cell characterization

A He-Ne beam ($\lambda = 632.8nm$) was launched with $\mathbf{k} \| z$ and focused at the cell entrance with a waist of about $6\mu m$. As for standard cells, the LCLV was provided with a suitably treated input glass plate to optimize beam coupling in the yz plane. Fig. 4.2 shows ordinary [fig. 4.2(a)], mixed [fig. 4.2(b)] and extraordinary [fig. 4.2(c),(d)] polarized beams in the unbiased cell, self-confinement being observed for the extraordinary wave at $P = 2mW$ [fig. 4.2(d)]. As the planar anchoring held the director at $\theta_0 = 45°$, we got $\delta \approx 7°$, consistent with the birefringence of E48.

As illustrated in fig.4.3, we varied V_{bias} and observed the beam evolution in the yz plane: we found that the Freederickszs transition took place for $V_{bias} = 2V$ (rms value); above this value, voltage-induced beam steering occurred and we evaluated the apparent walk-off (i.e. the observable angle between $\mathbf{s}$ and $\mathbf{k}$ in the yz plane): it progressively reduced until, for $V_{bias} = 10V$, the beam became nearly parallel to z. Above that voltage, due to out-of-plane propagation, beam bouncing at the surfaces prevented a correct evaluation of the trajectory. Noteworthy, for higher voltages the beam lost self-confinement because of the saturating nonlinearity, as apparent from the last photograph in fig. 4.3(a).

The next step was to enable the photoconductor response: a beam from a solid state laser at $\lambda = 532nm$ (within the absorption band of the BSO) was tailored by a controllable liquid crystal display (LCD) acting as a spatial light modulator, in order to

(a) **(b)**
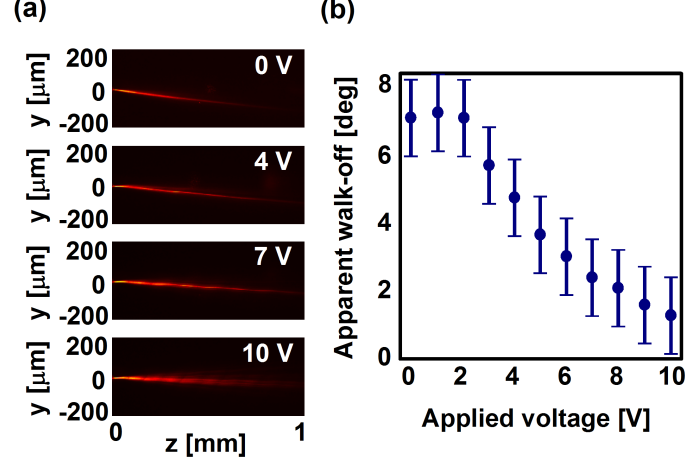
Figure 4.3: Beam propagation for various applied voltages. (a) Photographs of soliton evolution. High voltages saturate the nonlinear response and self-confinement is lost. (b) Apparent walk-off (projection of the actual walk-off on the yz plane) versus applied voltage.

obtain the desired shape and size, as sketched in fig. 4.1(a). We began with an expanded beam to have a uniform illumination $I(y, z) = S_c$; this way we induced a uniform linear and nonlinear response in the whole NLC. For a fixed voltage ($V_{bias} = 3.5V$) and intensity ($S_c = 0.25 mW/cm^2$), we first checked the frequency cut-off stemming from the equivalent capacitances of NLC and BSO layers and the BSO dispersion (fig. 4.4).
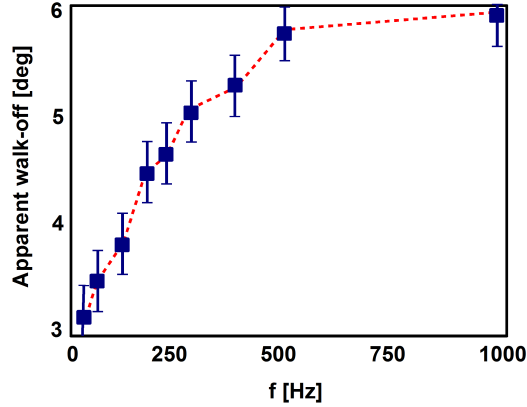
Figure 4.4: Frequency response of the LCLV. $V = 3.5V$(rms).

The apparent walk-off variations were evaluated for different values of the bias frequency. As expected, high frequencies were cut off by the cell and the nematicon

trajectory had negligible variations with respect to the unbiased cell. The cut-off frequency was found to be $f \approx 400Hz$; only below this value the photo-generated charges managed to affect the NLC reorientation, as witnessed by walk-off variations. The measured maximum BSO sensitivity resulted below $100Hz$. Thus, we set $f = 80Hz$ and studied the optical response of the LCLV, varying the impinging beam intensity for uniform illumination. The results are summarized in fig. 4.5: the soliton was angularly steered in the propagation plane, in analogy to what observed and reported in fig. 4.3, but by way of an optical control. As the flux S_c varied from 0 to $1mW/cm^2$, the walk-off varied linearly with an "equivalent" voltage dynamics from 3.5 to $8V$. The linear relation broke down above $S_c = 0.7mW/cm^2$ when saturation of the nematic response (walk-off nearly zero, as for the ordinary polarization) came into play.

From comparison between electric and optical responses of the valve we could estimate the parameters $\gamma = 0.6$ and $\alpha = 3 \cdot 10^3 V cm^2/W$, which are compatible with other measurements on LCLV with BSO. (82)
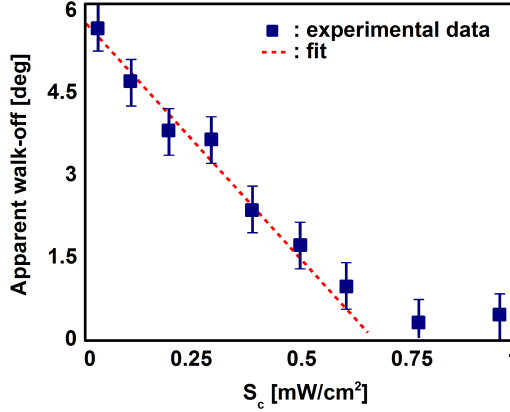
Figure 4.5: Optically induced soliton steering under uniform illumination. The linear trend of the apparent walk-off stops when the nonlinear response saturates. $V = 3.5V$(rms).

4.3   Nematicon propagation in LCLV: Model

The next step is the study of a nematicon propagating in a non-homogeneous NLC surrounding, as generated by shining beams of different shapes and sizes on the BSO. For the sake of simplicity, we refer to the effect of a round spot on a nematicon trajectory in yz, as shown in fig. 4.6: the soliton nearby the "defect" of the molecular director

[fig. 4.6(c)] is deviated towards its center.

Due to the spatial light modulator, flat-top control spots can be easily generated; the anchoring at the surfaces, combined with the external illumination, produces 3D perturbations in the LCLV. To model the effects of these perturbations we define two angles θ and φ [fig. 4.6(b)-(c)]: the former is the twist in yz as used in the previous chapters, the latter is the tilt in xz. The overall reorientation angles will be $\varphi = \varphi_{Vc} + \varphi_b$ and $\theta = \theta_{Vc} + \theta_b$, with $\varphi_{Vc} = \varphi_V + \varphi_c$ and $\theta_{Vc} = \theta_V + \theta_c$, the subscripts "V", "c" and "b" indicating the effects of voltage, control beam and soliton, respectively. We define the director "background" by considering the LCLV in the absence of solitons, i.e. $\theta_b = \varphi_b = 0$.
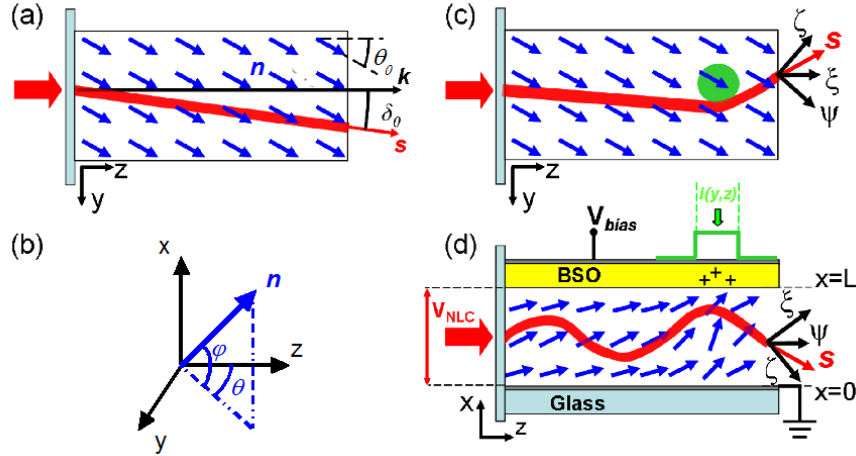
Figure 4.6: (a) Top view of a LCLV in the absence of control beam and with $V_{bias} = 0$. (b) Elevation and azimuth of the director $\boldsymbol{n}$ in xyz. (c) Top and (d) side views of an LCLV with a flat-top round control beam of intensity I and a soliton launched in $x = L/2$ with $\boldsymbol{k} \parallel z$. (c) and (d) show the projections of the moving reference $\xi\psi\zeta$ along the soliton (displayed in the output section). The (blue) arrows indicate the director distribution.

As the BSO dielectric constant [$\epsilon_{BSO} \approx 56$ (89)] is much larger than in NLC ($\epsilon_\parallel \approx 20$), the electric field components in yz plane are negligible and the reorientation due to a control spot occurs in the plane defined by x and the unperturbed $\boldsymbol{n}$: hence, $\theta = \theta_0$ owing to the boundary conditions and $\varphi = \varphi_0$, as stemming from the combined action of the voltage and the control beam. In these conditions we can cast the reorientation
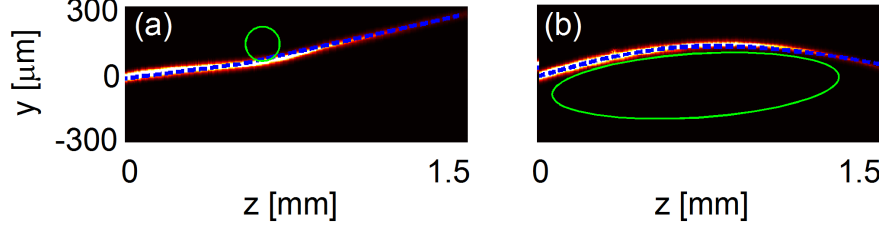
Figure 4.7: Nematicon in LCLV interacting with (a) circularly and (b) elliptically shaped spots. The blue dashed lines are trajectories derived from the theoretical model, in perfect agreement with the experiments.

equation [eq. (1.9)] as:

$$\nabla^2 \varphi_{Vc} + \kappa \sin(2\varphi_{Vc}) E_{NLC}^2 = 0 \tag{4.2}$$

where $E_{NLC} = V_{NLC}/L$, V_{NLC} is defined by eq. (4.1) and L is the cell thickness.

To compute the nematicon propagation through the director distribution $\mathbf{n}(x, y, z)$ defined by eq. (4.2) we assume $\theta_b << \theta_{Vc}$ and $\varphi_b << \varphi_{Vc}$, as the nonlinear perturbations are much smaller than the electric ones. (90) Since a typical nonlocality range $\approx 50\mu m$ ensures the validity of the Mauguin limit (33)(36), the changes in director can be taken adiabatic. Introducing a moving frame $\xi\psi\zeta$, with ζ parallel to the local wavevector $\boldsymbol{k}$, ξ the ordinary axis, $\psi\xi$ the principal plane of the extraordinary polarization and $\hat{\zeta} = \hat{\xi} \times \hat{\psi}$, the NLSE (eq. (1.8)) becomes:

$$2in_e k_0 \left[\frac{\partial^2 A'}{\partial \zeta^2} + \tan\delta(\zeta)\frac{\partial A'}{\partial \psi} \right] + \frac{1}{D_\zeta}\frac{\partial^2 A'}{\partial \xi^2} + \frac{D_\psi}{D_\zeta}\frac{\partial^2 A'}{\partial \psi^2} + k_0^2 \Delta n_e^2 A = 0 \tag{4.3}$$

where A' is the transverse electric field, Δn_e the space varying extraordinary index accounting for both optical and electrical reorientation, and $D_{\psi/\zeta}$ are the diffraction coefficients in the new reference system. Applying the Ehrenfest theorem and making use of the nonlocality, we obtain $2k_0^2 n_e^2 d^2\mathbf{r}_b/d\zeta^2 = \mathbf{F}|_{\mathbf{r}_b=\bar{\mathbf{r}}_b}$, $\mathbf{F}$ being the equivalent force depending on extraordinary refractive index changes and walk-off, as defined in previous chapters.

This model accounts for anisotropy, nonlinearity, nonlocality and nonhomogeneity in the full 3D setting. In fig. 4.7 two examples of nematicon propagation in the presence of "defects" are shown: circularly and elliptically shaped spots are considered

with flat-top profiles; due to the intensity $I = 0.16 mW/cm^2$ and the nonlocal response of the NLC, the corresponding angular profile saturates within the spot and is *sech*-like outside it. Noteworthy, an excellent agreement between the experimental and calculated trajectories is found.

4.4 All-optical signal processing in Liquid Crystals Light Valves

We managed how to control soliton paths in LCLV by exploiting the BSO response to external beams of given shapes. Thanks to the programmable spatial light modulator, we were able to shine on the photoconductor one or more *control spot(s)* and deviate the nematicon trajectory in a reconfigurable way. Thus, the LCLV is an ideal environment to achieve all-optical signal processing and routing. In the following we present some examples of soliton-based digital and analog functions in LCLV: we first define the *input/output* variables and the corresponding *states* in terms of measurable quantities.

We use as *input variables* the control spots on the BSO (in the examples $I = 100 \mu m/cm^2$): the *low state* (logic state 0) is associated to the absence of the spot, while the *high state* (logic state 1) applies when the spot is switched on by the spatial light modulator.

We consider as *output variable* the soliton y-position at a given z-section. When implementing de-multiplexing functions in space this association is straightforward, as the routed output can be defined as a spatial coordinate too. For logic functions, the output state is *high* when the nematicon position corresponds to a pre-determined location, *low* when the beam is deviated elsewhere. Thus, the design of a generic function is based on the spot position, size and shape, as they determine the soliton deviation.

4.4.1 Logic functions

4.4.1.1 Half-Adder

The basic element of a computer Central Processing Unit (CPU) is a Half-Adder, which yields the sum of two bits and provides the carry bit when needed. By tailoring the locations of two external spots in yz and weighting the two control bits on a nematicon in order to induce different deflections, a three-output binary Half-Adder can be implemented, as illustrated in fig. 4.8. If only one bit was *high* (i.e. logic input 10 or 01), the soliton was deviated from its straight trajectory (00 defined by V_{bias} and the birefringent walk-off) to the sum output S. Thus, the latter was at the *high* value (1) while the carry output C was low (0). The presence of both inputs (11) moved the soliton to the carry output C, bringing it to the *high* value and S to the *low* value.
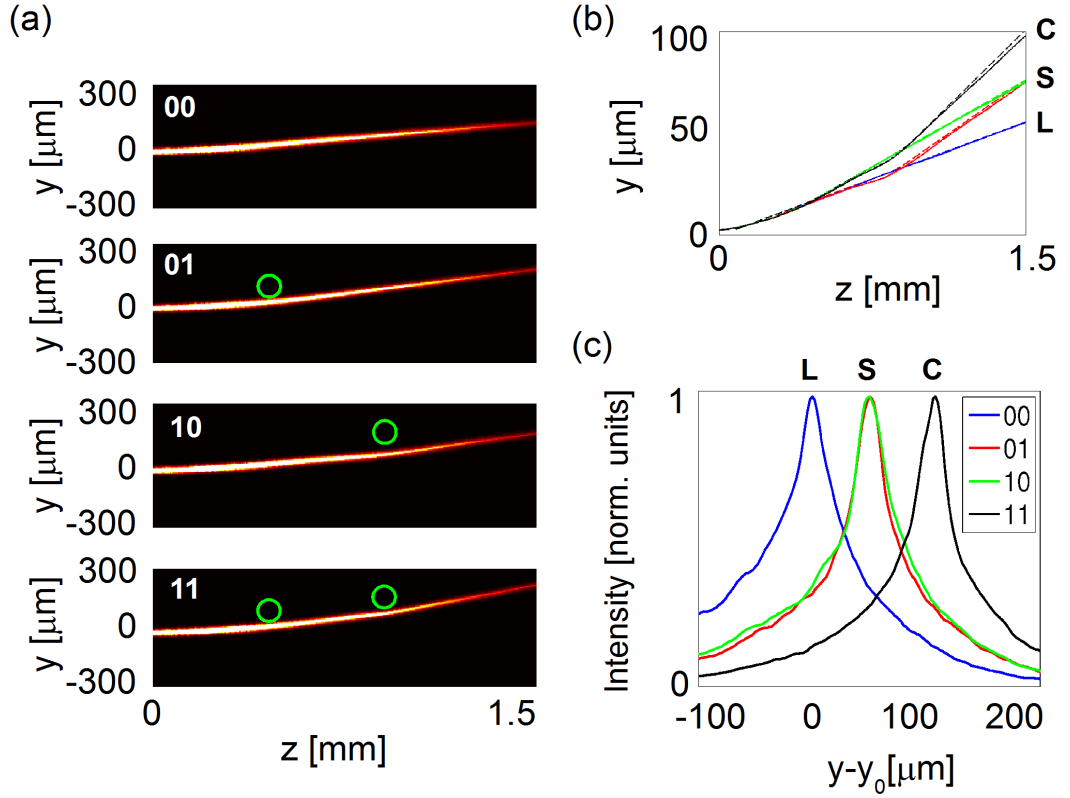
Figure 4.8: Realization of a Half-Adder. (a) Soliton propagation for various defect configurations, as indicated by the Boolean legends. The spots are centered in $[y,z] = [-100, 500]\mu m$ and $[y,z] = [-200, 900]\mu m$. Green circles represent the shape of the spots. (b) Soliton evolution in yz plane: acquired (solid lines) and model derived (dashed lines) trajectories; labels C, S, and L refer to *carry*, *sum* and *low-input*, respectively. (c) Transverse profiles in $z = 1.5mm$ corresponding to various logic outputs. y_0 is the output transverse position of the unperturbed nematicon (corresponding to input 00).

4.4.1.2 Logic gates

Configurations similar to the previously described system can implement the most common logic gates. The versatility of the soliton-deviation based system permitted to change function just assigning different variables to the output positions, leaving unaltered the "defect" arrangement.

Output C of the Half-Adder (fig. 4.8), for instance, is the output of an AND gate:
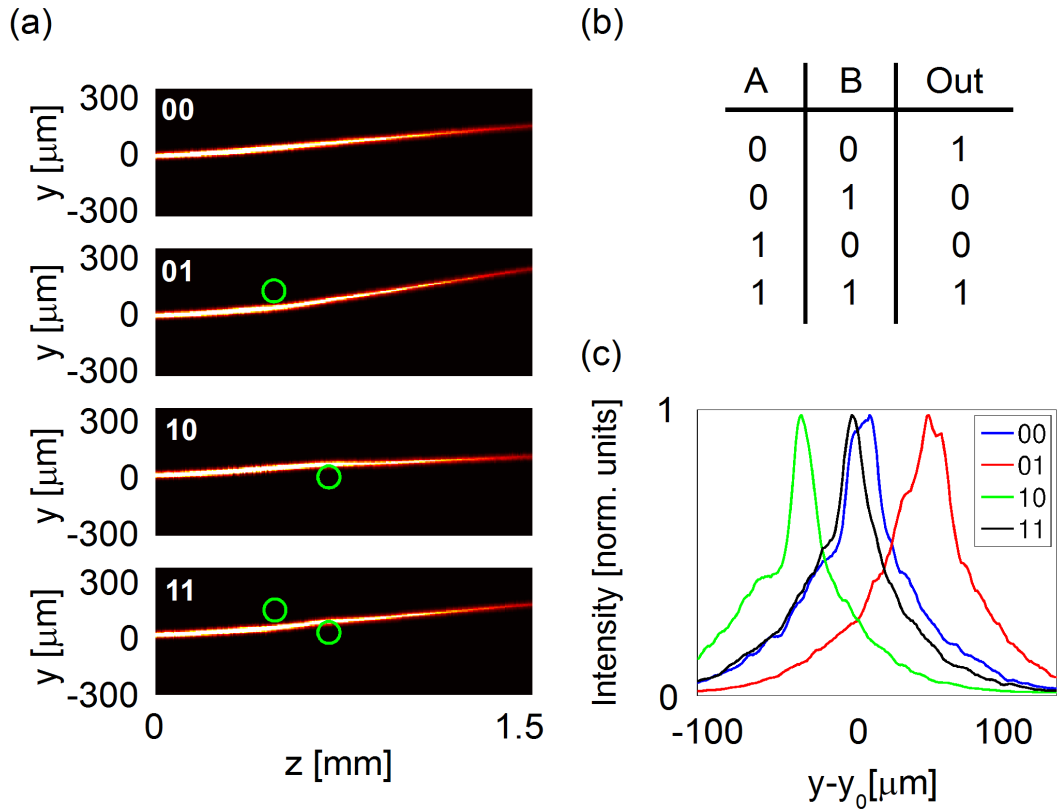
Figure 4.9: XNOR logic gate. (a) Soliton evolution in yz without and with control spots centered in $[y, z] = [-100, 500]\mu m$ and $[y, z] = [0, 700]\mu m$ for control inputs 01 and 10, respectively. Green circles are the spot edges. (b) Truth table of an XNOR. (c) Nematicon profiles in $z = 1.5mm$, with corresponding inputs. y_0 corresponds to the logic input 00

the *high* output state is associated to the 11 input state. Output S is the output of an XOR, the output value being *high* when the input bits are different (01 or 10). Finally, output L implements a NOR gate: the output is *high* just when all the inputs are low. In particular, NOR gates are universal, i.e. any logic function can be synthesized by their combination; hence, they are fundamental blocks for all-optical programmable

logic. By positioning differently the two control spots we could also obtain an XNOR gate (output *high* when the two input bits have the same value). The control spots were arranged to exactly compensated the two deviations, as clear from fig. 4.9.

4.4.2 Routing signals

As said earlier, the soliton deviation by the photo-induced defects can be easily associated to de-multiplexing functions. In fig. 4.10 an example of a programmable 1 x 4 demultiplexer is illustrated: every $(2^2 = 4)$ combination of Boolean inputs was able to re-route a spatial soliton (and the signal traveling within it) to a different output port.
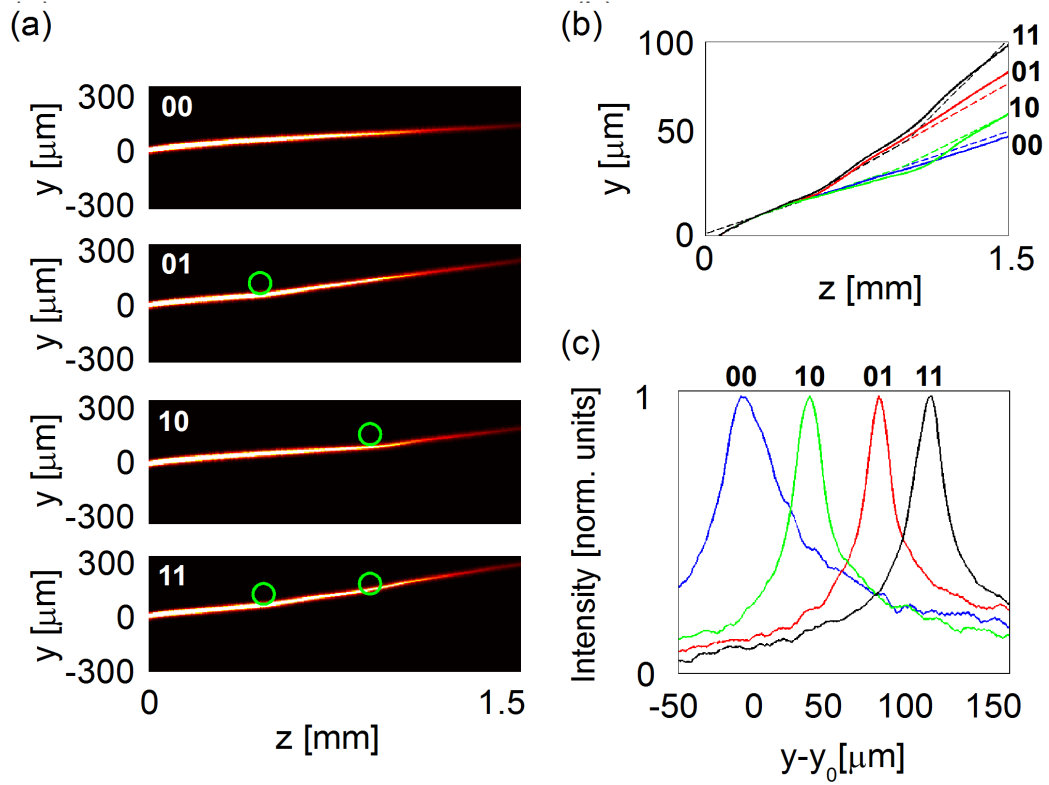
Figure 4.10: Two bit 1 x 4 router. (a) Photographs of soliton trajectories controlled by two control spots (circles), centered in $[y, z] = [-100, 500]\mu m$ and $[y, z] = [-150, 900]\mu m$. (b) Measured (solid lines) and simulated (dashed lines) nematicon trajectories. (c) Output profiles ($z = 1.5mm$) corresponding to the various inputs (Boolean legends). In (b), the solid and dashed lines refer to experiments and simulations, respectively. y_0 corresponds to the logic input 00.

(a)

(b)
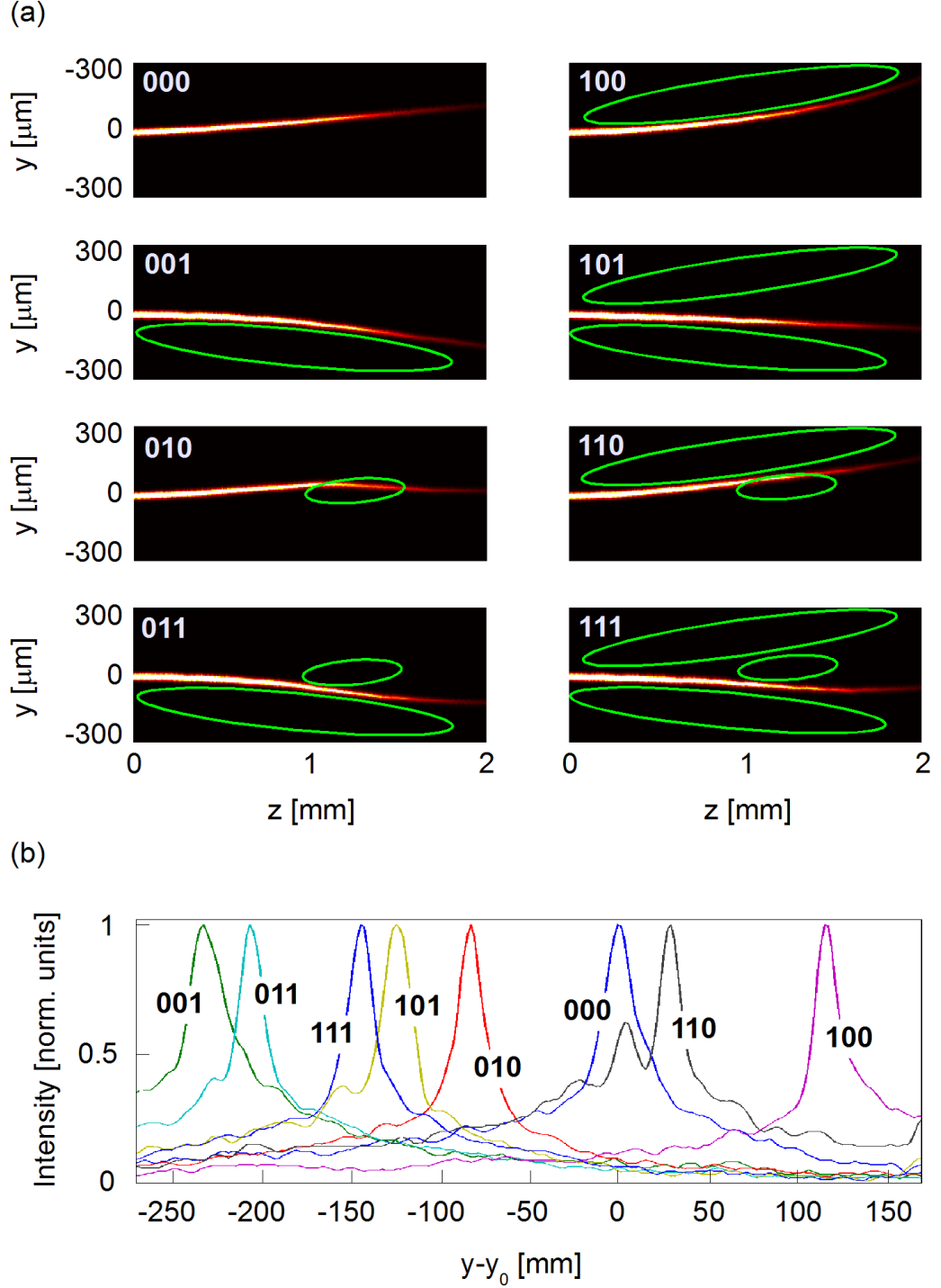
Figure 4.11: Three-bit 1 x 8 digital router controlled by elliptic external beams. (a) Photographs of soliton paths produced by the logic inputs in the legends. The closed lines point out the location and form of the control beams. Green ellipses correspond to the spots impinging on the BSO. (b) Output ($z = 2mm$) transverse profiles for the various Boolean inputs. y_0 corresponds to logic input 000.

A 3-bit all-optical router, i.e. a 1 x 8 demultiplexer, could be implemented by using control beams with suitable ellipticities and orientations to steer the soliton over a wide interval. The $(2^3 = 8)$ combinations of input bit let us distinguish eight different output positions over a transverse interval of $400 \mu m$, corresponding to a total angular range of $\approx 20°$, as visible in fig. 4.11.

4.4.3 Junctions

An external beam can also modulate the attraction between nematicons, implementing reconfigurable waveguide-based junctions as shown in fig. 4.12: two solitons with the same power, launched with parallel wavevectors and mutual separation larger than the non-locality range ($\approx 100 \mu m$), were pulled towards each other in the presence of a lens-like perturbation induced between them. Depending on position and shape of the control spot, the two solitons merged or interleaved, implementing optically-adjustable Y [fig. 4.12(b,d)] or X [fig. 4.12(c,e)] junctions, respectively.
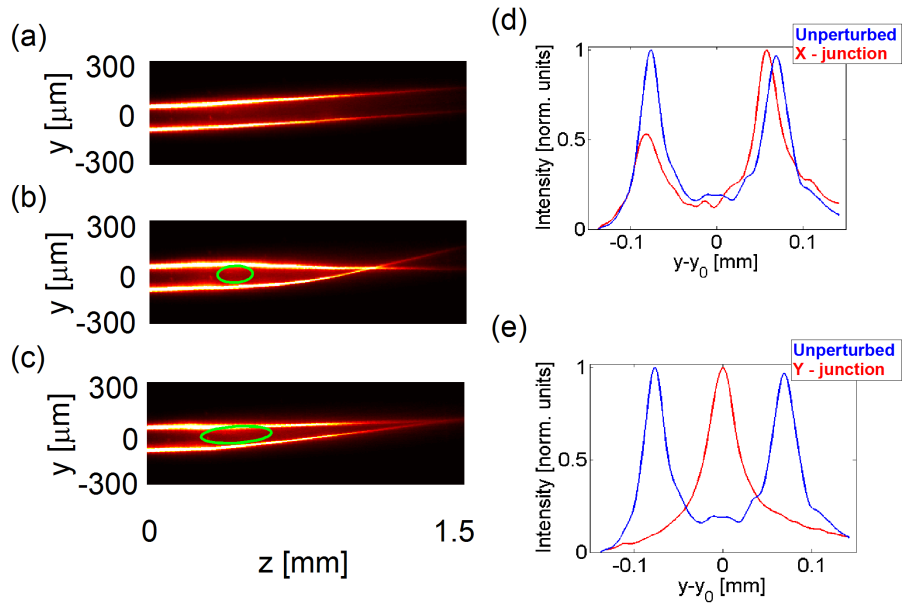
Figure 4.12: A two-soliton all-optical analog processor. Photographs of solitons (a) without and with a (b) round or (c) elliptical control beams imping on the LCLV. The green circle and ellipse represent the spot positions. (d-e) Transverse profiles corresponding to (b) X-junction or (c) Y-junction: the blue and red lines refer to unperturbed and deviated solitons, respectively. y_0 is the median position between the unperturbed nematicons at the output section.

4.5   Conclusions

We demonstrated the use of photoconductive LCLV as a versatile environment to control of one or more spatial solitons and the signals they transmit. An external illumination on the photoconductor side of the valve allowed shaping and controlling a number of lens-like index perturbations on the paths of the solitons, thereby enabling their routing in the whole space of propagation. The developed model permits to predict the trajectory, accounting for the peculiar 3D interactions between solitons and director landscape. The experimental set-up allowed us building a full set of all-optical signal processors: logic gates, as well as routers and junctions were demonstrated.

5

Discussions

In this dissertation I have discussed a few experiments on self-localized waves in nematic liquid crystals; by employing different sample geometries and materials I investigated the propagation of nematicons in both electrically and optically induced molecular director perturbations. All the phenomena, supported by suitable theoretical models, are milestones in the comprehension of propagation of solitons in nonlocal nonlinear media. I investigated a cell with a voltage-tunable nonlinearity, studying soliton trajectory and waist variations. The nonlocality-mediated interaction between two solitons was used to evaluate the angular momentum of a nonlinear system. Beam self-steering was studied in two different arrangements: in undoped NLC (avoiding instabilities) and in DDNLC, where the role of a non-negligible longitudinal field component was taken into account for the first time. Then, employing external beams, I addressed the effect of non-uniform director distributions: dye-induced defects were exploited to all-optical interfaces generation; LCLV provided an ideal platform to dynamically control nematicon paths. Particular attention has been devoted to the realization all-optical devices exploiting the above effects. Based on linearly- and nonlinearly-induced nematicon steering and bouncing, a number of strategies for signal processing and re-addressing, both in 2D and in 3D geometries, were proposed: soliton in-plane steering, soliton nonlinear spiraling, self-steering and dye-mediated optical interfaces are examples of de-multiplexing functions, while LCLV hosted a complete set of all-optical reconfigurable processors. Future work should address the realization of efficient input/output coupling strategies, in order to complete a soliton based system for all-optical parallel computing and/or signal routing.

Appendix A

Materials

A.1 Nematic Liquid Crystals

A.1.1 5CB - 4-Cyano-4'-pentylbiphenyl

5CB (4-Cyano-4'-pentylbiphenyl), chemical formula $C_{18}H_{19}N$ is the most common nematic liquid crystal. As sketched in fig. A.1, the molecule is about $2nm$ long, with a ratio between long and short axes of ≈ 10.
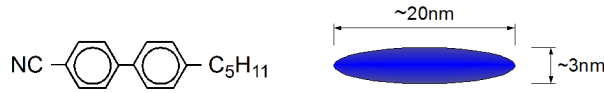
Figure A.1: Molecular structure and size of nematic 5CB.

The nematic-isotropic transition temperature is $T_{NI} = 36°C$. The extraordinary and ordinary refractive indices, for $\lambda = 1.064nm$ and $(T - T_{NI} = -10°C)$ are:

$$n_e = 1.6965$$

$$n_o = 1.5350$$

The elastic constants are:

$$K_1 = 6.2 \cdot 10^{-12} N$$

$$K_2 = 3.9 \cdot 10^{-12} N$$

$$K_3 = 8.2 \cdot 10^{-12} N$$

for splay, bend and twist deformations, respectively.

A.1.2 E7

E7 is a liquid crystalline mixture. Its molecular composition, illustrated in fig. A.2, was engineered to obtain a larger birefringence and a higher transition temperature $T_{NI} \approx 59°$ than 5CB:
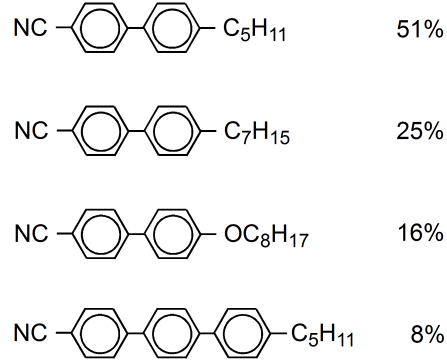
Figure A.2: Molecular structure of the E7 nematic mixture, with the relative composition.

The low frequency electric constants:

$$\epsilon_{\parallel} = 19.5$$

$$\epsilon_{\perp} = 5.1$$

For $T - T_{NI} = -10°C$ and λ=1064nm, the refractive indices are:

$$\lambda = 1064nm$$

$$n_e = 1.6954$$

$$n_o = 1.5038$$

$$\lambda = 442nm$$

$$n_e = 1.8129$$

$$n_o = 1.5426$$

And the Frank's constants:

$$K_1 = 12 \cdot 10^{-12} N$$

$$K_2 = 9 \cdot 10^{-12} N$$

$$K_3 = 19 \cdot 10^{-12} N$$

A.2 Dyes

A.2.1 1-Amino-Anthraquinone

1-Amino-Anthraquinone is an anthraquinone derivative, a natural dye compound. Dissolved in NLC it enables a thermal nonlinearity and enhances the reorientational one.
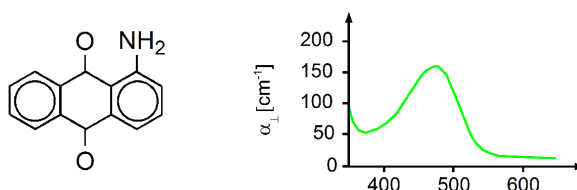
Figure A.3: Molecular structure and absorption spectrum of 1-AAQ.

A.2.2 Methyl Red

Methyl Red is an azo-dye, i.e. it suffers wavelength dependent molecular transitions, thus being responsible for several nonlinear effects when dissolved in NLC (from negative reorientational response to *Trans-Cis* transformation, adsorption/desorption on surfaces, etc.).
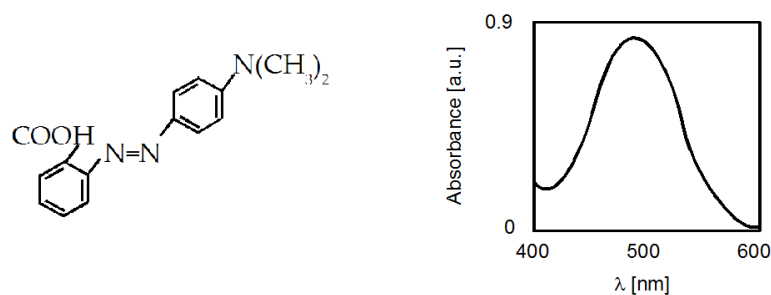
Figure A.4: Molecular structure and absorption spectrum of Methyl Red.

56

Appendix B

Liquid Crystals: cell technology

For some experiments, like the dye-induced self-steering and the LCLV, we fabricated the NLC samples. Here we report on the standard technology used to build the cells.

Properly cut glasses (coated with Indium Tin Oxide) were used as cell interfaces and washed in an ultrasonic bath with demineralized water. This removed impurities, preventing an inhomogeneous director distribution.

The molecular anchoring was realized on soft matter. Each inner surfaces was covered by a solution (2%) of dissolved *Polyvinyl alcohol* (PVA) and spinned to obtain a uniform thin layer. To optimize PVA adhesion on the ITO a soft baking was used.

Rubbing is a crucial process, as it allows NLC uniform anchoring and determines the initial director orientation in the overall sample, sometimes defining a pretilt. A velvet roll was used to lightly scratch the PVA: the NLC molecules laid with their long axes along the mechanically induced furrows. The process time was a compromise between the efficient generation of furrows and the removal of the PVA layer.

The sample was sealed with a UV glue; a careful up/down alignment of interfaces allowed the application of a third (rubbed) glass plate used as input facet. The separation (defining the cell thickness) was obtained with Mylar spacers. After sealing the cell, the NLC was infiltrated by capillarity. The uniform alignment could be checked under illumination between crossed polarizers.

Appendix C

Publications

C.1 Journals

- A. Fratalocchi, A. Piccardi, M. Peccianti and G. Assanto, "Nonlinearly controlled angular momentum of soliton clusters", *Opt. Lett.*, **32**, 1147 (2007)

- A. Fratalocchi, A. Piccardi, M. Peccianti and G. Assanto, "Nonlinear management of the angular momentum of soliton clusters: Theory and experiment", *Phys. Rev. A*, **75**, 063835 (2007)

- A. Piccardi, G. Assanto, L. Lucchetti and F. Simoni, "All-optical steering of soliton waveguides in dye-doped liquid crystals", *Appl. Phys. Lett.*, **93**, 171104 (2008)

- A. Piccardi, U. Bortolozzo, S. Residori and G. Assanto, "Spatial solitons in liquid-crystal light valves", *Opt. Lett.*, **34**, 737 (2009)

- A. Piccardi, M. Peccianti, G. Assanto, A. Dyadyusha and M. Kaczmarek, "Voltage-driven in-plane steering of nematicons", *Appl. Phys. Lett.*, **94**, 091106(2009)

- G. Assanto, A. Piccardi, A. Alberucci, U. Bortolozzo and S. Residori, "Liquid Crystal Light Valves: a versatile platform for Nematicons", *Phot. Lett. Pol.*, **1**, 151 (2009)

- A. Alberucci, A. Piccardi, U. Bortolozzo, S. Residori and G. Assanto, "Nematicon all-optical control in liquid crystal light valves", *Opt. Lett.*, **35**, 390 (2010)

- A. Piccardi, A. Alberucci and G. Assanto, "Soliton self-deflection via power-dependent walk-off", *Appl. Phys. Lett.*, **96**, 061105 (2010)

- A. Piccardi, A. Alberucci, U. Bortolozzo, S. Residori and G. Assanto, "Soliton gating and switching in liquid crystal light valve", *Appl. Phys. Lett.*, **96**, 071104 (2010)

- A. Piccardi, A. Alberucci, U. Bortolozzo, S. Residori and G. Assanto, "Readdrassable interconnects with spatial soliton waveguides in liquid crystal light valves", *Phot. Techn. Lett.*, *in press*

- G. Assanto, A. Piccardi, A. Alberucci, U. Bortolozzo and S. Residori, "Nematicons in Liquid Crystal Light Valves", *Mol. Crys. Liq. Cryst.*, *accepted*

- A. Piccardi, A. Alberucci and G. Assanto, "Self-turning self-confined light beams in a guest-host reorientational medium", *Phys. Rev. Lett.*, *submitted*

- A. Piccardi, A. Alberucci and G. Assanto, "Sub-mW dissipative nematicons and spontaneous light emission in dye-doped nematic liquid crystals", *Electr. Lett.*, *submitted*

C.2 Conferences

- A. Fratalocchi, A. Piccardi, M. Peccianti, and G. Assanto: "Nonlinear controlling the angular momentum of a solitary wave cluster", IQEC 2007, pap. ID3-4-FRI

- A. Piccardi and G. Assanto: "Nonlinear control of soliton spiraling", IEEE LEOS Annual Meeting 2007, pp. 620-1, Orlando (FL), Oct. 21-25, 2007

- A. Piccardi, M. Peccianti, and G. Assanto: "Non-Linear Control of Soliton Spiraling in Nematic Liquid Crystals", LEOS Winter Top. "Nonlinear Photonics", pp. 117-8, Sorrento (Italy), Jan. 14-16, 2008

- A. Piccardi, G. Assanto, L. Lucchetti and F. Simoni: "All-optical waveguide steering with spatial solitons in liquid crystals", First Mediterranean Photonics 2008, pp. 206-8, 25-28 June 2008, Ischia (Italy)

- G. Assanto, M. Peccianti, A. Alberucci and A. Piccardi: "Routing Light with Nematicons: Light Localization and Steering in Liquid Crystals", Int. Quantum Electron. Conf. IQEC 2009, Baltimore (USA), ITuG1, May 31-June 5, 2009 [Invited]

- U. Bortolozzo, A. Piccardi, S. Residori and G. Assanto: "Nematicons in Liquid Crystal Light Valves", Eur. Quantum Electron. Conf. EQEC 2009, pp. 1-1, June 14-19 2009

- G. Assanto, U. Bortolozzo, A. Piccardi, S. Residori and A. Alberucci: "A novel and versatile 3D setting for Nematicons: Liquid Crystal Light Valves", Int. Conf.: Opt. Liq. Cryst. OLC-2009, Erice (Italy), Sept. 28-Oct.2, 2009 [Invited]

- G. Assanto, A. Piccardi, S. Residori, U. Bortolozzo: "Liquid Crystal Light Valves: a versatile platform for Nematicons", Nonlinear Optics and Applications, Zakopane (PL), Sept. 23-26, 2009 [Invited]

- A. Alberucci, A. Piccardi and G. Assanto: "Self-bending Self-confined Light Beams", ACOFT/ACOLS 2009 (DS 2009), Adelaide (AU), Nov. 30, 2009 [Invited]

- U. Bortolozzo, S. Residori, A. Piccardi, A. Alberucci and G. Assanto: "Optically Reconfigurable Spatial Soliton Control and Gating in Liquid Crystal Light Valves", CLEO 2010, submitted

- A. Piccardi, A. Alberucci and G. Assanto: "Soliton self-deflection via power-dependent walk-off", OSA Nonlinear Photonics, Kalsruhe (Germany), June 21-24, 2010, submitted

- A. Piccardi, A. Alberucci, U. Bortolozzo, S. Residori, and G. Assanto: "Nematicon Routing in Liquid Crystal Light Valve", OSA Nonlinear Photonics, Kalsruhe (Germany), June 21-24, 2010, submitted

- A. Fratalocchi, A. Piccardi, M. Peccianti e G. Assanto: "Controllo nonlineare del momento angolare di cluster di solitoni", pp. 419-22, Fotonica 2007, Mantua, May 21-23, 2007

- A. Piccardi, A. Alberucci and G. Assanto: "Soliton self-steering via all-optical changes in walk-off", Fotonica 2010, Pisa (Italy), May 25-27, 2010 submitted

A. Alberucci, A. Piccardi and G. Assanto: "Self-turning of non-paraxial self-trapped light beams", Fotonica 2010, Pisa (Italy), May 25-27, 2010 submitted

- A. Piccardi, M. Peccianti and G. Assanto: "Voltage controlled in-plane steering of solitons", Fotonica 2010, Pisa (Italy), May 25-27, 2010 submitted

- A. Alberucci, A. Piccardi and G. Assanto: "Spatial Optical Solitons in Uniaxial Media", Fotonica 2010, Pisa (Italy), May 25-27, 2010 submitted

References

[1] E. Fermi, J. Pasta, and S. Ulam, "Studies of non linear problems," *Los Alamos National Laboratory*, Technical Report, 1955. 1

[2] P. A. Franken, A. E. Hill, C. W. Peters, and G. Weinreich, "Generation of optical harmonics," *Phys. Rev. Lett.*, vol. 7, no. 4, pp. 118–119, 1961. 1

[3] R. Y. Chiao, E. Garmire, and C. H. Townes, "Self-trapping of optical beams," *Phys. Rev. Lett.*, vol. 13, no. 15, pp. 479–482, 1964. 2, 4

[4] D. Grischkowsky, "Self-focusing of light by potassium vapor," *Phys. Rev. Lett.*, vol. 24, no. 16, pp. 866–869, 1970. 2

[5] J. E. Bjorkholm and A. A. Ashkin, "cw self-focusing and self-trapping of light in sodium vapor," *Phys. Rev. Lett.*, vol. 32, no. 4, pp. 129–132, 1974. 2, 4

[6] J. S. Russell, "Report on waves," in *Report of the fourteenth meeting of the British Association for the Advancement of Science*, York, September 1844 (London 1845), 1844, pp. 311–390. 2

[7] G. Stegeman, D. Christodoulides, and M. Segev, "Optical spatial solitons: historical perspectives," *IEEE J. Quantum Electron.*, vol. 6, no. 6, pp. 1419–1427, Nov/Dec 2000. 2, 3

[8] G. I. Stegeman and M. Segev, "Optical Spatial Solitons and Their Interactions: Universality and Diversity," *Science*, vol. 286, no. 5444, pp. 1518–1523, 1999. 3

[9] Y. S. Kivshar and G. P. Agrawal, *Optical Solitons.* San Diego, CA: Academic, 2003. 3

[10] A. S. Davidov, *Biology and quantum mechanics*. Oxford: Pergamon press, 1983. 3

[11] A. J. Heeger, S. Kivelson, J. R. Schrieffer, and W. P. Su, "Solitons in conducting polymers," *Rev. Mod. Phys.*, vol. 60, no. 3, pp. 781–850, 1988. 3

[12] A. R. Bishop and T. Schneider, *Solitons and condensed matter physics*. Berlin: Springer, 1978. 3

[13] N. J. Zabusky and M. D. Kruskal, "Interaction of 'solitons' in a collisionless plasma and the recurrence of initial states," *Phys. Rev. Lett.*, vol. 15, no. 6, pp. 240–243, 1965. 3

[14] S. Burger, K. Bongs, S. Dettmer, W. Ertmer, K. Sengstock, A. Sanpera, G. V. Shlyapnikov, and M. Lewenstein, "Dark solitons in Bose-Einstein Condensates," *Phys. Rev. Lett.*, vol. 83, no. 25, pp. 5198–5201, 1999. 3

[15] J. Denschlag, J. E. Simsarian, D. L. Feder, C. W. Clark, L. A. Collins, J. Cubizolles, L. Deng, E. W. Hagley, K. Helmerson, W. P. Reinhardt, S. L. Rolston, B. I. Schneider, and W. D. Phillips, "Generating solitons by phase engineering of a Bose-Einstein condensate," *Science*, vol. 287, p. 5450, 2000. 3

[16] M. J. Ablowitz and P. A. Clarkson, *Solitons, Nonlinear Evolution Equations and Inverse Scattering*. Cambridge: Cambridge University Press, 1991. 3, 4

[17] J. J. Sakurai, *Modern Quantum Mechanics*. Reading, MA: Addison-Wesley, 1994. 3, 19

[18] S. Trillo and W. E. Torruellas, *Spatial Solitons*. Berlin: Springer-Verlag, 2001. 3

[19] C. Conti and G. Assanto, *Encyclopedia of Modern Optics*. Oxford: Elsevier, 2004, vol. 5, ch. Nonlinear optics applications: Bright spatial solitons, pp. 43–55. 3

[20] Y. S. Kivshar and B. Luther-Davies, "Dark optical solitons: physics and applications," *Phys. Rep.*, vol. 298, pp. 81–197, 1998. 3, 4

[21] W. Krolikowski, O. Bang, J. J. Rasmussen, and J. Wyller, "Modulational instability in nonlocal nonlinear kerr media," *Phys. Rev. E*, vol. 64, p. 016612, 2001. 3

[22] O. Bang, W. Krolikowski, J. Wyller, and J. J. Rasmussen, "Collapse arrest and soliton stabilization in nonlocal nonlinear media," *Phys. Rev. E*, vol. 66, p. 046619, 2002. 3

[23] M. Peccianti, K. Brzadkiewicz, and G. Assanto, "Nonlocal spatial soliton interactions in nematic liquid crystals," *Opt. Lett.*, vol. 27, p. 1460, 2002. 3, 10

[24] A. W. Snyder and D. J. Mitchell, "Accessible solitons," *Science*, vol. 276, p. 1538, 1997. 4, 12, 18

[25] C. Conti, M. Peccianti, and G. Assanto, "Route to nonlocality and observation of accessible solitons," *Phys. Rev. Lett.*, vol. 91, p. 073901, 2003. 4, 9, 10

[26] ——, "Observation of optical spatial solitons in a highly nonlocal medium," *Phys. Rev. Lett.*, vol. 92, p. 113902, 2004. 4, 9, 12, 14

[27] W. E. Torruellas, Z. Wang, D. J. Hagan, E. W. VanStryland, G. I. Stegeman, L. Torner, and C. R. Menyuk, "Observation of two-dimensional spatial solitary waves in a quadratic medium," *Phys. Rev. Lett.*, vol. 74, no. 25, pp. 5036–5039, 1995. 4

[28] C. Rothschild, B. Alfassi, O. Cohen, and M. Segev, "Long-range interactions between optical solitons," *Nature Phys.*, vol. 2, p. 769, 2006. 4, 18

[29] F. Derrien, J. F. Henninot, M. Warenghem, and G. Abbate, "A thermal (2D+1) spatial optical soliton in a dye doped liquid crystal," *J. Opt. A: Pure Appl. Opt.*, vol. 2, p. 332, 2000. 4

[30] M. Segev, B. Crosignani, A. Yariv, and B. Fischer, "Spatial solitons in photorefractive media," *Phys. Rev. Lett.*, vol. 68, p. 923, 1992. 4

[31] M. Peccianti, C. Conti, G. Assanto, A. DeLuca, and C. Umeton, "Routing of anisotropic spatial solitons and modulational instability in nematic liquid crystals," *Nature*, vol. 432, p. 733, 2004. 4, 9, 10

[32] G. Assanto and M. Peccianti, "Spatial solitons in nematic liquid crystals," *IEEE J. Quantum Electron.,*, vol. 39, no. 1, pp. 13–21, Jan 2003. 4, 9

[33] P. G. DeGennes and J. Prost, *The Physics of Liquid Crystals.* New York: Oxford Science, 1993. 4, 6, 9, 31, 32, 44

[34] I. C. Khoo, *Liquid Crystals: Physical Properties and Nonlinear Optical Phenomena.* New York: Wiley, 1995. 5, 7

[35] F. Simoni, *Nonlinear Optical Properties of Liquid Crystals.* Singapore: World Scientific, 1997. 5, 10

[36] A. Alberucci, M. Peccianti, G. Assanto, G. Coschignano, A. DeLuca, and C. Umeton, "Self-healing generation of spatial solitons in liquid crystals," *Opt. Lett.*, vol. 30, no. 11, pp. 1381–1383, 2005. 8, 44

[37] B. Alfassi, C. Rotschild, O. Manela, M. Segev, and D. N. Christodoulides, "Boundary force effects exerted on solitons in highly nonlocal nonlinear media," *Opt. Lett.*, vol. 32, p. 154, 2006. 8

[38] A. Alberucci, M. Peccianti, and G. Assanto, "Nonlinear bouncing of nonlocal spatial solitons at the boundaries," *Opt. Lett.*, vol. 32, p. 2795, 2007. 8

[39] ——, "Propagation of optical spatial solitons in finite size media: interplay between non locality and boundary conditions," *J. Opt. Soc. Am. B"*, vol. 24, p. 2314, 2007. 8

[40] M. Peccianti, A. DeRossi, G. Assanto, A. DeLuca, C. Umeton, and I. C. Khoo, "Electrically assisted self-confinement and waveguiding in planar nematic liquid crystal cells," *Appl. Phys. Lett.*, vol. 77, no. 1, pp. 7–9, 2000. 9, 12

[41] N. Tabiryan and B. Zeldovich, "The orientational optical nonlinearity of liquid-crystals," *Mol. Cryst. Liq. Cryst.*, vol. 62, pp. 237–250, 1980. 9

[42] E. Braun, L. P. Faucheux, and A. Libchaber, "Strong self-focusing in nematic liquid crystals," *Phys. Rev. A*, vol. 48, no. 1, pp. 611–622, 1993. 9

[43] C. Conti, M. Peccianti, and G. Assanto, "Spatial solitons and modulational instability in the presence of large birefringence: the case of highly non-local liquid crystals," *Phys. Rev. E*, vol. 72, p. 066614, 2005. 9

[44] M. Peccianti and G. Assanto, "Incoherent spatial solitary waves in nematic liquid crystals," *Opt. Lett.*, vol. 26, p. 1791, 2001. 10

[45] M. Peccianti, C. Conti, G. Assanto, A. DeLuca, and C. Umeton, "All optical switching and logic gating with spatial solitons in liquid crystals," *Appl. Phys. Lett.*, vol. 81, p. 3335, 2002. 10

[46] A. Pasquazi, A. Alberucci, M. Peccianti, and G. Assanto, "Signal processing by opto-optical interactions between self-localized and free propagating beams in liquid crystals," *Appl. Phys. Lett.*, vol. 87, no. 26, p. 261104, 2005. 10, 33

[47] S. V. Serak, N. V. Tabiryan, M. Peccianti, and G. Assanto, "Spatial soliton all-optical logic gates," *IEEE Photon. Techn. Lett.*, vol. 18, p. 1287, 2006. 10, 24, 33

[48] M. Peccianti, G. Assanto, A. Dyadyusha, and M. Kaczmarek, "Tunable refraction and reflection of self-confined light beams," *Nature Phys.*, vol. 2, pp. 737 – 742, 2006. 10

[49] ——, "Non-specular total internal reflection of spatial solitons at the interface between highly birefringent media," *Phys. Rev. Lett.*, vol. 98, p. 113902, 2007. 10, 12

[50] ——, "Nonlinear shift of spatial solitons at a graded dielectric interface," *Opt. Lett.*, vol. 32, no. 3, pp. 271–273, 2007. 10

[51] M. Peccianti, C. Conti, and G. Assanto, "The interplay between non locality and nonlinearity in nematic liquid crystals," *Opt. Lett.*, vol. 30, p. 415, 2005. 12

[52] M. Peccianti, A. Fratalocchi, and G. Assanto, "Transverse dynamics of nematicons," *Opt. Express*, vol. 12, p. 6524, 2004. 12

[53] A. V. Buryak and V. V. Steblina, "Soliton collisions in bulk quadratic media: comprehensive analytical and numerical study," *J. Opt. Soc. Am. B*, vol. 16, pp. 245–255, 1999. 18

[54] A. S. Desyatnikov and Y. S. Kivshar, "Rotating optical soliton clusters," *Phys. Rev. Lett.*, vol. 88, p. 053901, 2002. 18

[55] M. Shih, Z. Chen, M. Segev, T. H. Coskun, and D. Christodoulides, "Incoherent collisions between one-dimensional steady-state photorefractive screening solitons," *Appl. Phys. Lett.*, vol. 69, p. 27, 1996. 18

[56] E. DelRe, S. Trillo, and A. J. Agranat, "Collisions and inhomogeneous forces between solitons of different dimensionality," *Opt. Lett.*, vol. 25, p. 560, 1999. 18

[57] A. Stepken, F. Kaiser, and M. R. Belić, "Anisotropic interaction of three-dimensional spatial screening solitons," *J. Opt. Soc. Am. B*, vol. 17, pp. 68–77, 2003. 18

[58] M. Shih and M. Segev, "Incoherent collisions between two-dimensional bright steady-state photorefractive spatial screening solitons," *Opt. Lett.*, vol. 21, p. 1538, 1996. 18

[59] C. Simos, V. Couderc, A. Barthélémy, and A. V. Buryak, "Phase-dependent interactions between three-wave spatial solitons in bulk quadratic media," *J. Opt. Soc. Am. B*, vol. 20, pp. 2133–2141, 2003. 18

[60] I. Jánossy, A. Lloyd, and B. Wherrett, "Anomalous optical freedericksz transition in an absorbing liquid crystal," *Mol. Cryst. Liq. Cryst.*, vol. 179, pp. 1–12, 1990. 23

[61] A. V. Yatsenko, V. V. Chernyshev, and A. L. A. H. Schenk, "1-aminoanthraquinone: Crystal data and a model of molecular packing," *Powder Diffr.*, vol. 13, p. 85, 1998. 23

[62] I. Jánossy, L. Csillag, and A. D. Lloyd, "Temperature dependence of the optical fréedericksz transition in dyed nematic liquid crystals," *Phys. Rev. A*, vol. 44, no. 12, pp. 8410–8413, 1991. 23

[63] I. Jánossy and A. D. Lloyd, "Low-power optical reorientation in dyed nematics," *Mol. Cryst. Liq. Cryst.*, vol. 203, p. 77, 1991. 23

[64] I. Jánossy and T. Kósa, "Influence of anthraquinone dyes on optical reorientation of nematic liquid crystals," *Opt. Lett.*, vol. 17, no. 17, pp. 1183–1185, 1992. 23

[65] S. Residori, G. Russo, S. McConville, and A. Petrosyan, "Surfactant controlled light induced reorientation in dye-doped nematic liquid crystals," *Mol. Cryst. Liq. Cryst.*, vol. 429, pp. 111–132, 2005. 23, 24

[66] I. C. Khoo, H. Li, and Y. Liang, "Optically induced extraordinarily large negative orientational nonlinearity in dye-doped liquid crystal," *IEEE J. Quantum Electron.*, vol. 29, no. 5, p. 1444, 1993. 23

[67] T. Kósa and I. Jánossy, "Anomalous wavelength dependence of the dye-induced optical reorientation in nematic liquid crystals," *Opt. Lett.*, vol. 20, no. 11, pp. 1230–1232, 1995. 23, 24

[68] I. Jánossy, "Molecular interpretation of the absorption-induced optical reorientation of nematic liquid crystals," *Phys. Rev. E*, vol. 49, no. 4, pp. 2957–2963, 1994. 23, 24

[69] L. Marrucci, D. Paparo, P. Maddalena, E. Massera, E. Prudnikova, and E. Santamato, "Role of guest-host intermolecular forces in photoinduced reorientation of dyed liquid crystals," *J. Chem. Phys.*, vol. 107, no. 23, pp. 9783–9793, 1997. 24

[70] L. Marrucci, D. Paparo, M. R. Vetrano, M. Colicchio, E. Santamato, and G. Viscardi, "Role of dye structure in photoinduced reorientation of dye-doped liquid crystals," *J. Chem. Phys.*, vol. 113, no. 22, pp. 10 361–10 366, 2000. 24

[71] C. Manzo, D. Paparo, S. Lettieri, and L. Marrucci, "Fluorescence-based investigation of the Janossy effect anomalous wavelength dependence," *Mol. Cryst. Liq. Cryst.*, vol. 421, pp. 145–155, 2004. 24

[72] M. Warenghem, J. F. Henninot, and G. Abbate, "Bulk optical Freedericksz effect: Non linear optics of nematics liquid crystals in capillaries," *Mol. Cryst. and Liq. Cryst.*, vol. 320, pp. 207–230, 1998. 24

[73] M. K. E. Benkler, I. Janossy, "Control of the orientational nonlinearity through photoisomerization in dye doped nematics," *Mol. Cryst. Liq. Cryst.*, vol. 375, pp. 701–711, 1992. 24

[74] E. Ouskova, Y. Reznikov, S. Shiyanovskii, L. Su, J. West, O. Kuksenok, O. Frances-
cangeli, and F. Simoni, "Photo-orientation of liquid crystals due to light-induced
desorption and adsorption of dye molecules on an aligning surface," *Phys. Rev. E*,
vol. 64, no. 5, p. 051709, 2001. 24, 34

[75] M. Warenghem, J. F. Henninot, F. Derrien, and G. Abbate, "Thermal and orien-
tational 2D+1 spatial optical solitons in dye doped liquid crystals," *Mol. Cryst.
and Liq. Cryst.*, vol. 373, pp. 213 – 225, 2002. 24

[76] M. Peccianti, C. Conti, E. Alberici, and G. Assanto, "Spatially incoherent modu-
lational instability in a nonlocal medium," *Laser Phys. Lett.*, vol. 2, p. 25, 2005.
27

[77] Y. Y. Yakovlev, R. N. Nurmukhametov, V. G. Klimenko, and N. N. Barashkov,
"Absorption and luminescence of amino- and benzoylaminoanthraquinones," *J.
Appl. Spectr.*, vol. 53, pp. 930–935, 1990. 31

[78] O. Francescangeli, S. Slussarenko, F. Simoni, D. Andrienko, V. Reshetnyak, and
Y. Reznikov, "Light-induced surface sliding of the nematic director in liquid crys-
tals," *Phys. Rev. Lett.*, vol. 82, no. 9, pp. 1855–1858, 1999. 33

[79] D. Fedorenko, E. Ouskova, V. Reshetnyak, and Y. Reznikov, "Evolution of light-
induced anchoring in dye-doped nematics: Experiment and model," *Phys. Rev. E*,
vol. 73, no. 3, p. 031701, 2006. 34

[80] J. A. van Raalte, "A new schlieren light valve for television projection," *Appl.
Opt.*, vol. 9, no. 10, pp. 2225–2230, 1970. 38

[81] J. D. Margerum, J. Nimoy, and S. Y. Wong, "Reversible ultraviolet imaging with
liquid crystals," *Appl. Phys. Lett.*, vol. 17, no. 2, pp. 51–53, 1970. 38

[82] S. Residori, "Patterns, fronts and structures in a liquid-crystal-light-valve with
optical feedback," *Phys. Rep.*, vol. 416, pp. 201–272, 2005. 38, 39, 42

[83] M. G. Clerc, A. Petrossian, and S. Residori, "Bouncing localized structures in a
liquid-crystal light-valve experiment," *Phys. Rev. E*, vol. 71, no. 1, p. 015205, 2005.
38

[84] U. Bortolozzo, R. Rojas, and S. Residori, "Spontaneous nucleation of localized peaks in a multistable nonlinear system," *Phys. Rev. E*, vol. 72, no. 4, p. 045201, 2005. 38

[85] U. Bortolozzo, A. Montina, F. T. Arecchi, J. P. Huignard, and S. Residori, "Spatiotemporal pulses in a liquid crystal optical oscillator," *Phys. Rev. Lett.*, vol. 99, no. 2, p. 023901, 2007. 38

[86] S. Residori, U. Bortolozzo, and J. P. Huignard, "Slow and fast light in liquid crystal light valves," *Phys. Rev. Lett.*, vol. 100, no. 20, p. 203603, 2008. 38

[87] P. Gunter and J. P. Huignard, *Photorefractive materials and their application 1*. Oxford: Springer, 2006. 39

[88] A. E. Attard, "Photoconductive and photorefractive effects in BSO," *Appl. Opt.*, vol. 28, p. 5169, 1999. 39

[89] P. Aubourg, J. P. Huignard, M. Hareng, and R. A. Mullen, "Liquid crystal light valve using bulk monocrystalline Bi12SiO20 as the photoconductive material," *Appl. Opt.*, vol. 21, p. 3706, 1982. 39, 43

[90] M. Peccianti, C. Conti, G. Assanto, A. DeLuca, and C. Umeton, "Nonlocal optical propagation in nonlinear nematic liquid crystals," *J. Nonl. Opt. Phys. Mat.*, vol. 12, p. 525, 2003. 44